# Power ultrasound-assisted enhancement of granulated blast furnace slag reactivity in cement paste

Paweł Lisowski [*], Daria Jóźwiak-Niedźwiedzka, Magdalena Osial, Kamil Bochenek, Piotr Denis, Michał A. Glinicki [**]

*Institute of Fundamental Technological Research Polish Academy of Sciences, Pawinskiego 5b, 02-106, Warsaw, Poland*

## ARTICLE INFO

## ABSTRACT

This paper introduces a first-time investigation into the impact of power ultrasound (PUS)-assisted preparation on the physicochemical and mechanical properties of cement-granulated blast furnace slag (GBFS) composite pastes. Pastes containing deposited GFBS with varying particle size fractions, partially replacing Portland cement, were prepared using PUS (ultrasonic horn tip, 20 kHz, 700 W) in pulse mode in a vertical jacketed glass sonoreactor with closed-circuit cooling. Cement paste incorporating 20 wt.% GBFS as mass substitution with varying particle size fractions was characterized by several physicochemical techniques at different curing ages. Exploring the cement and GBFS interaction induced by PUS, the compressive and flexural strength, the elastic modulus and indentation hardness, the heat of hardening, the mineral composition of hydration products, and the specific surface area BET were evaluated for a curing time of up to 28 days. The grain size distribution of GFBS and the reaction mixture's pH were measured. Both mechanical properties, heat of hydration and nano-porosity exhibited strong sensitivity to PUS treatment. Sonofragmentation of GBFS particles (especially the 125–250 μm fraction) increased with increasing sonication time, resulting in a relative increase of fraction <63 μm and a decrease of fraction >125 μm by 275 % and 60 %, respectively. Using the obtained SEM-EDS data, a simplified mechanism is proposed to explain the effects induced by PUS treatment.

## 1. Introduction

Lately, there has been considerable scientific and environmental discourse surrounding the concept of utilizing supplementary cementitious materials (SCMs) in place of Portland cement (PC) clinker to mitigate the consumption of natural resources and reduce $CO_2$ emissions during cement production [1–3]. In particular, a solid industrial by-product like GBFS has become extensively used either as one of the main constituents of multicomponent cement or as an active mineral additive to the concrete mix [3,4]. For GBFS blended cement concrete, improved physicochemical and durability properties were observed, e.g. Refs. [5,6]. The diminishing availability and escalating expense of high-quality GBFS, as well as the slower early hardening that contributes to a reduction in performance at early ages, are some of the drawbacks of

concrete technology with such an addition to the concrete mix [4–9]. As a result, a lot of attention has been devoted to enhancing the early-age performance of cement-based materials, which may answer the requirements of concrete production for the rapid erection of buildings, precast product manufacturing, and road repairs.

The strength of cement-GBFS materials cannot generally be reliably predicted, despite developing multiple indices based on chemical and physical parameters to predict GBFS reactivity [4]. GBFS glass dissolution significantly affects the slag hydration process, particularly in the early stages [10]. An almost impenetrable layer of hydrated calcium and aluminosilicate deficiency is quickly created on the surface of GBFS grains by the GBFS reaction with $H_2O$ [4,10–13]. In most cases, only the presence of activators causes the concentration of $OH^-$ ions to rise and this coating to break down, accelerating the reaction [4,10–13].

Efficient grinding can increase the intrinsic activity of GBFS, but finer grinding mainly improves medium and late strength, with a limited impact on the early strength that is governed by the lower hydration rate of GBFS [4,10–14].

Apart from the fineness, various factors elucidated in the literature [4,10–21] affect slag's reactivity in cement systems. Slag hydrates more slowly than cement clinker, with its hydration facilitated by the alkaline medium provided by accelerated clinker hydration. The amorphous phase's chemical composition and pore solution characteristics affect slag reactivity. Studies indicate that calcium ions inhibit slag dissolution, while aluminium presence decreases slag reaction rates. Furthermore, the chemical composition of slag, particularly its MgO and $Al_2O_3$ contents, affects its reactivity [4,10–22]. Alumina content influences the formation of different phase assemblages in high-alumina slag cement. Anionic species like sulfates and calcite play a significant part in the pore solution because they affect how alumina is mixed with hydrates and where the hydrates are distributed. The interaction between anionic species in composite cement is clarified by studies on simplified systems containing carbonates, calcium hydroxide, and sulphates [14]. Aluminate-bearing hydration products precipitate more quickly with sulphates than with carbonates, which only moderately accelerate slag dissolution. The microstructure and elemental hydration product analysis reveal insights into the factors controlling slag reactivity, indicating that a combination of macro-capillary pore space and anionic species influence slag hydration in ternary cements.

PUS treatment has demonstrated interesting potential for enhancing dispersion in cementitious systems and influencing cement-based materials' characteristics [23–32,36,37]. Previous publications revealed beneficial effects of PUS on the dispersion of densified silica fume and natural pozzolans in cementitious systems (disaggregation and dispersion of particle clusters), observed to lead to better pozzolanic activity [25–27]. Ehsani et al. [33] described the beneficial impacts of PUS on the fc and fr of hardened Portland cement mortar: after 91 days of hardening the strength increased by as much as 7 % and 11 %, respectively. Stronger sonication effects on the concrete's early strength development [34] could be achieved by adjusting the sonication parameters (amplitude and energy). The PUS-induced degassing effect resulted in the removal of the entrapped air voids in cement suspensions and hardened cement pastes, thus improving the resulting mechanical properties [19,28]. Tricalcium silicate paste hydration was shown to be significantly impacted by PUS treatment [35], which caused heterogeneous C-S-H nucleation and CH right after sonication. Xiong et al. [39] revealed that early and late-age fc of cement paste improved by 26 % at 1 d and 18 % at 28 d. The C-S-H gel's mean chain length increased with increasing ultrasonic power, and PUS-assisted mixing resulted in refined capillary and gel pores. A pore solution composition study [29] revealed higher concentrations of Al on ultrasonic processing, suggesting that the higher availability of Al during hydration may lead to the formation of C–S–H with higher Al. However, some contradicting results were reported for moderate (0.5) and elevated (0.8) w/c ratios [29]. Inexplicable differences in the PUS influence on the composition of cement hydration products (portlandite content, degree of hydration) are found. Some differences could be associated with the sonication technique, particularly the unknown effectiveness of the cooling circuit, possibly resulting in substantially elevated temperatures of sonicated mixtures and predominantly thermal effects.

The published studies failed to identify the PUS effects on the hydration of SCMs, and GBFS activity under PUS treatment was not reported in the literature. Deposited and coarse GBFS was not specifically studied. Remus et al. [40] reported preliminary results of PUS-assisted preparation of blended cements containing GBFS (20 % CEM I + 80 % CEM II/B-S), claiming a carbon emission reduction of 30 %, preserving the early strength. In this case, ground GFBS served as a component of CEM II/B-S cement (21–35 % by weight according to EN 197-1 standard), and the acceleration effects were obtained from the pre-hydrated cement suspension's seeding effect. Not only does the effectiveness of

PUS on GBFS-cement systems call for further investigation, but also the soundness of test conditions to diminish data discrepancies needs to be addressed.

The novelty of this study in comparison to previous studies on PUS in cement systems comprises the improved sonication technique with an efficient cooling system to control the mixture temperatures which allows for advancement in the recognition of PUS effects on the hydration and strength development of cement systems with granulated blast-furnace slag. The sonication technique was optimized to increase the efficiency of the sonofragmentation of GBFS particles. GFBS activity in cement systems under PUS treatment has not been previously reported in the literature.

The objective of this study is to reveal the influence of PUS treatment on the physicochemical and mechanical characteristics of cement-GBFS paste while using deposited and fractionated granulated blast-furnace slag. The selection of GFBS for the current study was influenced both by desired environmental benefits and the potential of PUS recognized within the area of chemical engineering. As known from numerous studies, PUS is effective in managing the rapid crystallization processes and generating a rapid nucleation rate ("sonocrystallization") [38,39] as well as particle size refinement ("sonofragmentation") [39,40]. Our working hypothesis is then derived that PUS treatment might exert a beneficial influence on rather coarse (non-finely ground) slag particles to improve their activity in cementitious systems. To achieve the reproducible and thermally controlled test conditions, a dedicated jacketed sonoreactor was applied with the cooling water circulation control by an ultrathermostat.

## 2. Experimental

### 2.1. Materials

Table 1 shows the chemical composition of PC (CEM I 42.5R) and GBFS. The main clinker minerals in cement have an estimated content of 66.5 % $C_3S$, 6.2 % $C_2S$, 7.9 % $C_3A$, and 8.6 % $C_4AF$ according to Bogue equations [41,42]. The glass phase content in GBFS (XRF analysis) is 89.8 % and 89.7 % for the fraction <63 μm and the fraction 125–250 μm, respectively. It exceeds a common requirement for a main constituent of blended cement according to European standards EN 15167–1:2006 (minimum glass phase content by mass not less than 67 %). The hydration modulus HM=(CaO + MgO + $Al_2O_3$)/$SiO_2$ and basicity coefficient Kb=(CaO + MgO)/($SiO_2$+$Al_2O_3$) of GBFS were found to be 1.6 and 1.1, respectively. GBFS originated from a deposit at a steel plant, and its bound water content was 1.2 %.

### 2.2. Specimen preparation procedure

The reference mixture of ordinary PC paste (denoted C) was prepared

**Table 1**
Chemical composition (%) of PC (CEM I 42.5 R) and GBFS determined by XRF analysis.

| Compound | CEM I 42.5 R | GBFS |
|---|---|---|
| $SiO_2$ | 19.542 | 37.568 |
| $Al_2O_3$ | 4.754 | 8.805 |
| $Fe_2O_3$ | 2.830 | 0.350 |
| CaO | 61.736 | 42.071 |
| MgO | 3.206 | 7.925 |
| $SO_3$ | 3.137 | 1.355 |
| $K_2O$ | 0.900 | 0.476 |
| $Na_2O$ | 0.161 | 0.507 |
| $P_2O_5$ | 0.120 | 0.007 |
| $TiO_2$ | 0.233 | 0.325 |
| $Mn_2O_3$ | 0.170 | 0.582 |
| LOI | 3.080 | 0.030 |
| Total | 100 | 100 |

at a 0.50 w/c ratio. Cement pastes with 20 wt.% of cement replaced by GBFS (denoted C + S) with different particle sizes (<63 μm, 63–125 μm, and 125–250 μm) were prepared at the same w/c ratio (see Appendix, Table A1). Paste mixtures were mixed using a mortar mixer according to PN-EN 196-1. At identical proportions of constituents, the pastes were also prepared using PUS-assisted mixing at different PUS exposure times (from 5 to 15 min.) with a continuous ultrasonic pulse mode (5s ON pulse time and 5s OFF - relaxation pulse time) to prevent overheating. Fig. 1 shows a PUS-assisted mixing system. Fig. 2 provides an example of the specific coding of different paste mixes.

Ultrasonic treatment of an aqueous reaction mixture was performed with a commercial vertical-type sonicator (QSonica 700, 20 kHz, 700 W, Newtown, USA). A vertical jacketed glass sonoreactor (diameter of 130.0 mm) was used for the preparation. The cooling water flow from an ultrathermostat was circulated through the sonoreactor jacket to reduce the temperature during PUS (measured by a thermocouple) and prevent overheating of the aqueous reaction mixture from unacceptable temperatures around 50 °C to ambient temperature (~23 °C) during specimen preparation and kept constant to avoid water evaporation (see Appendix, Table A2). The ultrasonic horn tip (diameter of 25.4 mm) was centrally located in sonoreactor and remained constant throughout each preparation. The sonication parameters were established experimentally during a preliminary investigation (see Appendix, Table A3, and Table A4).

Prepared fresh CP was molded into horizontal prismatic molds (25 × 25 × 140 mm) at room temperature, compacted using a vibrating table, and kept under tight cover for 24 h at the laboratory at 20–23 °C and an RH of 60–70 %, then de-molded and cured in the $H_2O$ at 20–23 °C for 2, 7, and 28 d, or until testing.

### 2.3. Methods of characterization

#### 2.3.1. Isothermal calorimetry method

A multichannel isothermal calorimeter (Calmetrix I-Cal 2000 HPC) was used to determine the progress of the prepared specimens' hydration. The thermostatic chamber was equilibrated for at least 12 h to reach a stable temperature of 23 °C before the isothermal test began, and the release of hydration heat was recorded continuously until 168 h.

#### 2.3.2. The substitute initial (IS) and final setting (FS) time

The IS and FS of the reference mixture of CP and CP with 20 wt.% of cement replaced by GBFS with different particle sizes were attempted using a standard Vicat's apparatus. The elevated w/c ratio (0.5), which is also the initial w/c ratio required to obtain an aqueous reaction mixture and perform PUS, hindered the achievement of reproducible
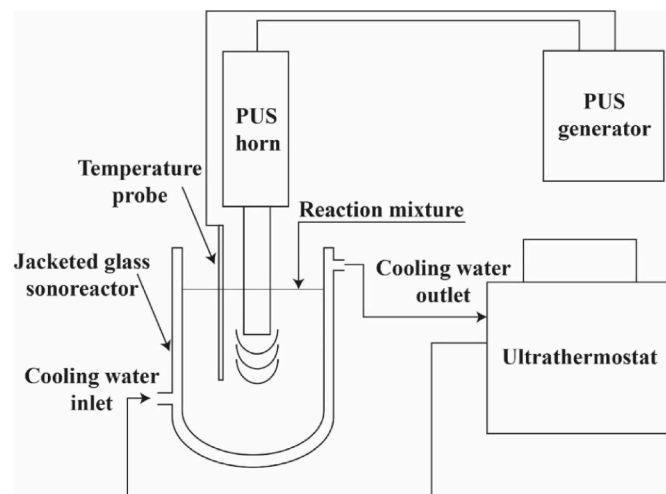


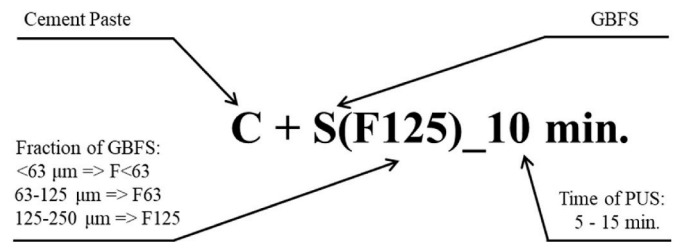**Fig. 1.** System for the preparation of specimens.



**Fig. 2.** Code for cement paste mixtures.

and reliable IS and FS times. The Vicat apparatus is well designed for cement paste of normal consistency (w/c ratio ≈ 0.3), and is therefore not so well suited for high w/c ratios, according to Ref. [43]. Lowering the w/c ratio below 0.5 during PUS may cause the ultrasonic converter to overheat, resulting in the pitting of the PUS probe tip, which could lead to cross-contamination, damage, or wear beyond its useable life. In this case, the substitute IS and FS times were determined by taking the first derivative of the function of the rate of heat generation in time during the isothermal calorimetry test. The detailed procedure is described in Ref. [44] which is based on [45].

#### 2.3.3. Laser granulometric analysis (LG)

The Malvern Mastersizer 3000 particle size analyser, coupled with the HydroMV2000, was used to define particle size distribution (PSD). Each test involved 500 mg of prepared materials. Isopropanol was used as the dispersion medium.

#### 2.3.4. The reaction mixture's pH

The reaction mixture's pH was checked initially and after PUS treatment by a SevenExcellence Mettler Toledo pH Meter.

#### 2.3.5. Depth-sensing microindentation method

Prior to microindentation testing, the prepared specimens (25 × 25 × 140 mm) were sliced into smaller halves (10 × 25 × 40 mm). The specimens' surfaces were carefully polished with abrasive papers to achieve a very smooth and flat surface, similar to those used for microscopic investigation. The debris and dust left on the specimens' surfaces were removed with compressed air. To avoid excessive expansive stresses and microcrack formation, specimens were not subjected to severe thermal differentials. Details concerning the apparatus and the experimental setting have been provided elsewhere [46]. For each specimen, the microindentation mapping results are the average of at least 15 measurements.

#### 2.3.6. Scanning electron microscope (SEM) equipped with an X-ray energy dispersion (EDS)

The specimens for SEM-EDS analysis were sliced into smaller halves (10 × 25 × 40 mm), dried (40 °C for 3 days for a constant weight), vacuum-impregnated with a low-viscosity epoxy resin, ground on diamond discs, then polished with diamond pastes on polishing pads. Following surface preparation, the specimens were dried for 3 d at 40 °C for constant weight, then coated with a carbon layer, and a strip of conductive tape was attached to them to enhance their conduction qualities. Each of the specimens was examined using a JEOL JSM-6460LV microscope with an EDS detector. The working distance and acceleration voltage of the SEM analysis were 10 mm and 20 kV, respectively.

#### 2.3.7. The compressive ($f_c$)/flexural strength ($f_r$) and hydration stoppage procedure

The $f_c$ and $f_r$ were determined on three prismatic specimens (25 × 25 × 140 mm) after 2, 7, and 28 d using the Automax Controls Pro Automatic model 50-C46Z00 (Italy). After the $f_r$ test, half of the prismatic specimens were used for the $f_c$ determination, and immediately after, the

representative crushed pieces of each specimen after 28 d were subjected to a strict procedure to stop further hydration, as recommended by RILEM [47]. Briefly, crushed pieces passed through a 1.00 mm sieve and then were immersed in an appropriate quantity and time of anhydrous isopropanol (purity ≥99.9 %) and anhydrous diethyl ether (purity ≥99.8 %). After rinsing and drying each sample in an oven with ventilation at 40 °C for 8 min, the dried specimens were put inside airtight plastic bags and enclosed in a desiccator with a low vacuum (~10 mbar) over silica gel (maximally protected from the hydration process) until further examination (XRD, TGA, FTIR, BET).

### 2.3.8. The compressive ($f_c$)/flexural strength ($f_r$) of mortar specimens

Cement mortars were prepared according to the European standard EN 196-1 with and without sonication treatment using standard siliceous sand, and the proportions are presented in Table A5 (see Appendix). The preparation of mortars marked with (US) was modified: the cement paste with GBFS was sonicated and then mixed with CEN sand according to EN 196-1 after sonication. In addition, the consistency of freshly mixed mortars was determined using EN 1015-3. The flexural and compressive strength of mortar was determined using standard specimens 40 × 40 × 160 mm after 2, 7, and 28 days of moist curing at 20 °C.

### 2.3.9. X-ray diffraction (XRD)

For X-ray diffraction (XRD) scans, a Bruker D8 Discover diffractometer was used with a Cu lamp source as a source (λ = 1.5418 Å), 40 kV voltage, and 40 mA current. Coupled theta/2theta geometry was used, 1 mm linear slit, with 1600W nominal operating power. Soller slits were used for both primary and secondary beam sides to increase resolution and reduce divergence of the beam. The measurement step size was 0,02°, with 1s counting time per step. Diffraction patterns were collected in a 2θ range from 10° to 70° with a 0,02° step, 1s counting time, using coupled θ-2θ geometry. Data evaluation was performed using Diffrac EVA 5.2 software, with the 2018 COD database embedded.

### 2.3.10. Thermogravimetric analysis (TGA)

The samples' thermogravimetric analysis (TGA) (minimum sample weight: 50 mg of the powder-like sample) was performed using a PerkinElmer TGA 8000 analyzer (Shelton, USA). It was measured from 35 °C to 1000 °C in an $N_2$ flow with a balance purge flow of 40 mL min$^{-1}$ and a heating rate of 20 °C min$^{-1}$. The recommended boundary conditions (e.g., amount of samples, heating rate, $N_2$ flow rate) for conducting TGA analysis were used from Ref. [48].

### 2.3.11. Fourier transform infrared spectroscopy (FTIR)

FTIR measurements were carried out using Bruker Vertex70 equipment in ATR mode (Bruker Platinum Diamond ATR stage, 8 scans averaged with 2 cm e$^{-1}$ resolution). Background scans were done before sample scans to as accurately as possible compensate for humidity and carbon-dioxide in-air content changes and subtracted automatically. In one sequence, all scans were done in ambient conditions of approximately 25 °C and 40 % relative humidity.

### 2.3.12. BET method

The SSA$_{BET}$ of the prepared specimens was performed using a Quantachrome Autosorb IQ analyser ($N_2$ adsorptive gas analysis) with a view to the Brunauer–Emmett–Teller (BET) method with the BJH model. To eliminate any moisture or other volatile contaminants, the process consisted of adding around 0.2 g and degassing for 16 h at 378.2 K under vacuum. Following degassing, BET measurements were carried out while the tubes were immersed in a liquid nitrogen bath at 77.3 K.

## 3. Test results

### 3.1. Compressive and flexural strength

Fig. 3a, 3b, and 3c (cement-GBFS paste specimens with variable slag particle sizes) show relationships between $f_c$ and $f_r$ and the impact of PUS treatment on cement and cement-slag pastes at different curing ages. After 2 d, the PC paste under 10 min. of PUS (C_10 min.) demonstrated the highest value of $f_c$ and $f_r$ among all cement-GBFS paste specimens under investigation.

After sonication treatment, the early compressive and flexural strengths of the cement-GBFS paste containing slag particles of 125–250 μm (C + S(F125)_10 min.) were quite similar to the reference paste. Without PUS, the early strengths of reference paste were relatively higher, approximately by 131.5 % and 58.1 % for the compressive and flexural strengths, respectively. In comparison to the cement-GBFS paste specimen with slag particles of <63 μm prepared without PUS, the early $f_c$ was increased by 96.1 %, and the $f_r$ was increased by 95.2 % due to 10 min. PUS treatment.

After 28 d, the $f_c$ and $f_r$ of C + S(F125)_10 min. considerably increased among all tested specimens (54.5 % and 50.7 % greater than C + S(F125) prepared without PUS). At the same age of curing, prepared specimens with PUS had higher $f_c$ and $f_r$ than prepared specimens without PUS, indicating that PUS treatment can be used as an effective strengthening method to improve the strength of reduced-clinker cement paste specimens.

The strength of mortar specimens determined at 2, 7, and 28 days of hardening is given in Table A5 (see Appendix). The early age strength development of mortar in time is illustrated in the Appendix in Fig. A1. This relative strength is determined in relation to the 28-day compressive strength prepared without PUS. Slump flow results for mortar mixtures are shown in Table A4 (see Appendix).

### 3.2. Depth-sensing microindentation

The prepared specimens' elastic modulus, as well as the indentation hardness, were examined using the multiple depth-sensing microindentation technique, and the results are shown in Fig. 4. A strong reduction of Vickers hardness (VH) and elastic modulus (EM) is seen due to partial replacement of cement by GBFS, by about 50 % and 65 %, respectively. As a result of PUS treatment, the average values of VH and EM for Portland cement paste were slightly increased (by 4–5%), but the increase was insignificant considering the data scatter. However, the effects of PUS on slag blended pastes were much stronger – it resulted in a relative rise of VH and EM by about 106 % and 72 %, respectively. After sonication treatment, the hardness and elastic modulus of cement-GBFS paste were in the range of 73–88 % of the respective average values for the reference paste. The relative effects of sonication treatment are quite similar to its effects on the strength ($f_c$ and $f_r$).

### 3.3. Hydration heat

The kinetics of heat evolution during isothermal hardening of cement pastes is shown in Fig. 5. Pastes prepared with PUS treatment (Fig. 5b) exhibited an elevated first exothermic peak (during the pre-induction period [19,49–54]) probably because of extended equilibration time, therefore, the initial 60 min. hardening period is excluded from the analysis. The peak of heat emission rate is observed after 116.5-135.5 min. after the start of measurements. Effects of cement dilution by GFBS are reflected by some reduction of heat emission rate and flattening of the main hydration rate peak, followed by some extension of the deceleration phase. The cumulative emitted heat curves (Fig. 5) demonstrate at each hardening stage a reduced total heat generated by GFBS-containing paste in comparison to the reference paste. This observation is relevant to specimens prepared without PUS treatment and similarly reflects the effect of cement dilution by GFBS.
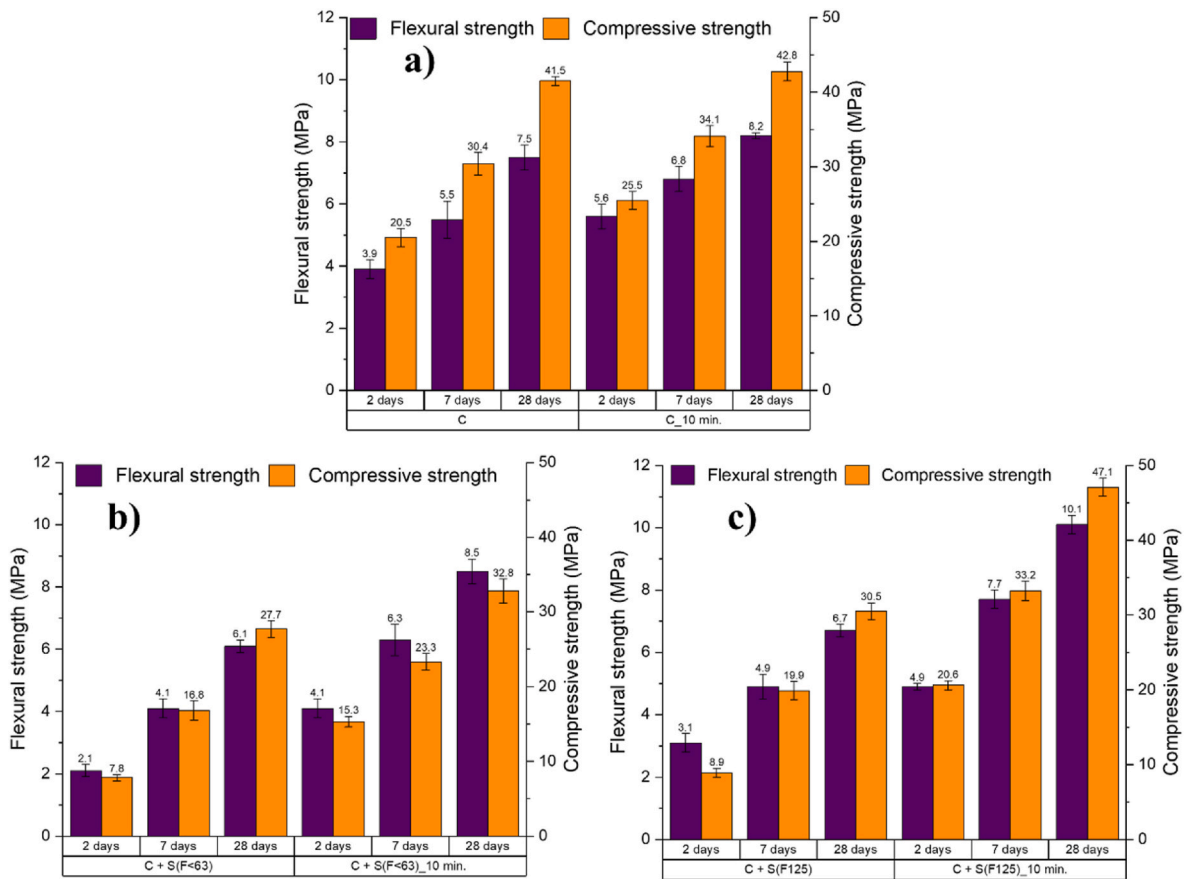
**Fig. 3.** $f_c$ and $f_r$ of hardened cement pastes at different curing times: a) no slag addition, b) 20 wt.% of GBFS with particles <63 μm, c) 20 wt.% of GBFS with particles 125–250 μm.
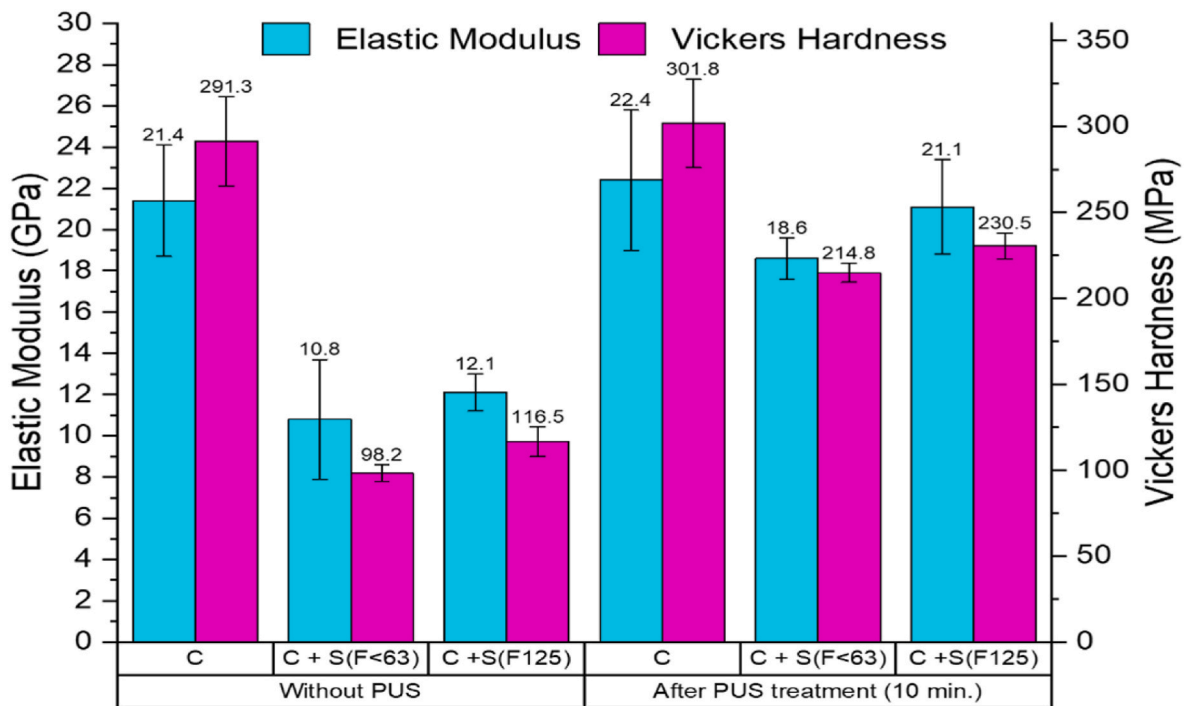


**Fig. 4.** The VH and EM of C + S pastes prepared conventionally and with the use of PUS after 28 d.
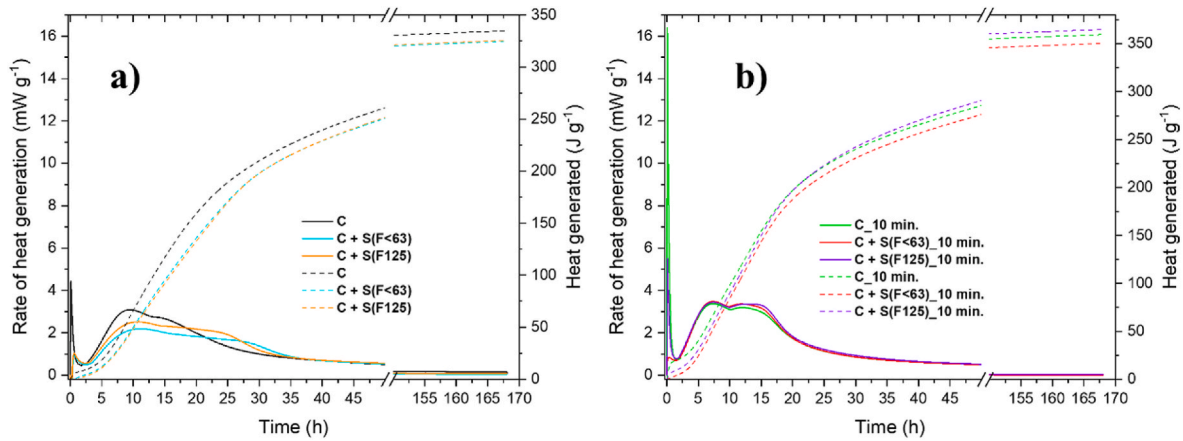
**Fig. 5.** Heat evolution during hydration of C + S pastes prepared conventionally (a) and with the use of PUS treatment (b).

Due to PUS treatment, the heat emission rate is increased, and the maximum heat rate is observed for the hardening time of 115.0–121.5 min. The shape of the heat rate curve becomes quite close for paste irrespective of its composition, counteracting the previously mentioned cement dilution effect. The total heat emitted during paste hardening (Table 2) is relatively increased due to PUS treatment by a factor within the range of 1.07–1.34. The highest relative increase is observed for the first 24-hour period.

For a clear demonstration of observed PUS effects, the cumulative heat data were normalized with respect to the total heat emitted during 168 h by reference cement paste. Such relative heat development data is shown in Fig. 6 – the differences between the blue and red lines demonstrate the effects of power ultrasound treatment. The parameters of the best-fit curves displayed as dotted lines are found to be the same for sonicated pastes C and C + S(F125).

The substitute initial and final setting times estimated using the heat rate curves are shown in Fig. 7. The effect of PUS treatment is consistent – a relative reduction of IS and FS is observed, by 22–24 % and by 24–39 %, respectively.

Comparing the calorimetric curves for cement pastes containing GBFS with different sizes prepared under the influence of PUS, it can be stated that the hydration kinetics slow down generally when the size of GBFS is < 63 μm, which may be connected with the sonofragmentation of GBFS particles. Sonofragmentation of GBFS (<63 μm) can generally be linked to the incapacity of the GBFS particles to retain the mixing water as they gravitationally descend downhill. On the other hand, during PUS treatment, partial stiffening of CP in the high-energy cavitation zone or on the surface of the sonoreactor wall, as well as local sedimentation of GBFS particles, can occur rapidly due to the mechanical impacts of acoustic cavitation bubbles. This indicates that during the pre-induction period, the GBFS (<63 μm fraction) sonofragmentation is

small and largely unaffected by filler effects. Additionally, the mixture exhibits very little overall exothermic activity, which makes rearranging and reorganizing the GBFS particles challenging. The preceding findings showed that the PUS may improve cumulative heat released and assessment of IS/FS and the reactivity of prepared specimens with various $SSA_{BET}$ (Table 5), which may cause an increment in the pre-induction period's rate (especially for 125–250 μm of GBFS particle size fractions).

*3.4. Thermal analysis*

The content of the hydration products of prepared specimens was semi-quantified using TGA analysis. The TG/DTG curves (Fig. 8) reveal three major mass loss stages during the heating process of prepared paste specimens. The first stage, from ambient to 260 °C, refers to the dehydration of C-S-H and ettringite, as well as the evaporation of $H_2O$ [55–57]. The range's second stage of 430–550 °C is associated with de-hydroxylation of CH [55–58]. The range's third stage of 550–1000 °C arose from the de-carbonation of $CaCO_3$ [55–57].

For the quantitative evaluation of the content of hydration products, the following formulas were applied to DTG and TG data. formula (1) was used to express the amount of CH as a percentage of the dry specimen weight at 550 °C [55–58]:

$$CH \ (wt.\%) = \frac{m_{CH}}{m_{550}} * \frac{74}{18} * 100 \tag{1}$$

The CH peak corresponds to the weight differential ($m_{CH}$) as calculated by the tangential method [55–58]. Using a 74/18 fraction, the CH-bound water was converted into CH mass. The relative reduction of CH content due to PUS treatment was determined using the modified formula (2) proposed by Rodríguez et al. [59]:

$$Reduction \ of \ the \ content \ of \ CH = \left( \frac{CH - CH_{PUS}}{CH} \right) * 100 \tag{2}$$

The CH content is found to be reduced by PUS treatment (Table 3). The highest reduction in CH content (29.4 %) was found concerning C + S(F125)_10 min., which can be linked to the creation of C-S-H/C-A-S-H seed via pozzolanic interactions between GBFS and Ca(OH)$_2$. Moreover, the area of deconvolution attributed to the C-S-H/ettringite phases for the PUS-treated Portland cement paste is smaller than the corresponding area for the paste prepared without PUS. This could result from a possible enhancement of the dissolution rate of the aluminate phase in the OPC clinker, as suggested previously in Ref. [29].

In general, $SiO_2$ and $Al_2O_3$ will react with CH crystals and produce C-S-H nucleation seeds due to the pozzolanic activity of GBFS; hence, the amount of CH in the hardened pastes decreases when GBFS is present [22,60–62]. Consequently, reduced CH content implies that more GBFS

**Table 2**
Heat development during paste hardening.

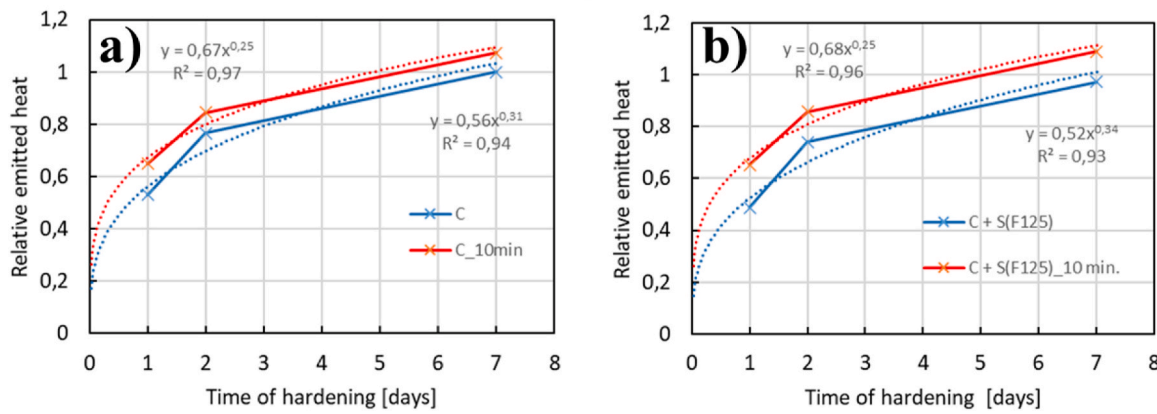| Cement paste composition and PUS treatment | Heat generated (J g$^{-1}$) | | |
|---|---|---|---|
| | 24 h | 48 h | 168 h |
| C | 178.8 ± 1.2 | 257.0 ± 1.3 | 335.0 ± 2.5 |
| C_10 min. | 218.0 ± 1.6 | 281.8 ± 1.5 | 359.7 ± 3.1 |
| C + S(F < 63) | 164.5 ± 1.4 | 246.8 ± 1.6 | 324.7 ± 3.0 |
| C + S(F < 63)_10 min. | 208.8 ± 1.9 | 272.5 ± 1.8 | 350.1 ± 3.3 |
| C + S(F125) | 163.0 ± 1.5 | 247.8 ± 1.6 | 325.7 ± 3.1 |
| C + S(F125)_10 min. | 218.6 ± 1.8 | 287.1 ± 1.7 | 364.9 ± 3.2 |

**Fig. 6.** The relative emitted heat during paste hardening for cement paste without and with PUS treatment of: a) reference cement paste, b) cement paste with GFBS fraction 125–250 μm.
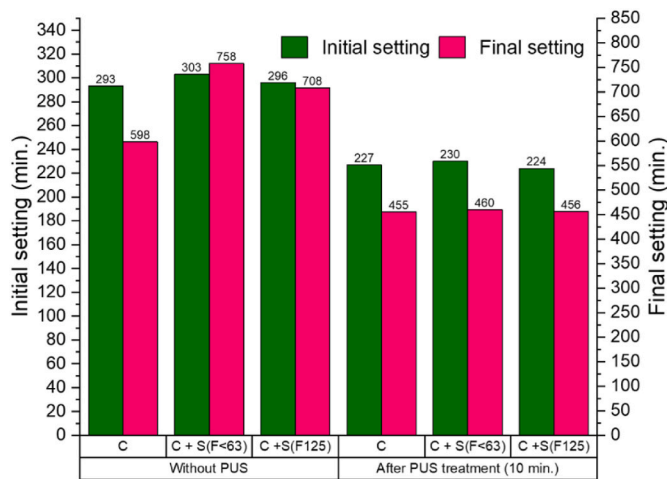


**Fig. 7.** Substitute IS and FS time for specimens of C + S pastes prepared conventionally and with the use of PUS treatment.

**Table 3**
CH content of cement pastes after 28 d.

| Composition and PUS treatment | Reduction of CH content [%] |
| --- | --- |
| C | 11.5 |
| C_10 min. | |
| C + S(F < 63) | 24.3 |
| C + S(F < 63)_10 min. | |
| C + S(F125) | 29.4 |
| C + S(F125)_10 min. | |

**Table 4**
Relative PSD of slag fraction (F125) after PUS treatment.

| PUS treatment | Relative mass content (%) | | | LG mode (μm) | | | Span (−) |
| --- | --- | --- | --- | --- | --- | --- | --- |
| | <63 μm | 63–125 μm | >125 μm | $D_{10}$ | $D_{50}$ | $D_{90}$ | |
| S(F125)_none | 100 | 100 | 100 | 91.3 | 205.0 | 352.0 | 1.26 |
| S(F125)_5 min. | 87.9 | 218.9 | 80.7 | 76.2 | 164.0 | 322.0 | 1.50 |
| S(F125)_10 min. | 274.9 | 245.4 | 60.1 | 23.0 | 126.0 | 233.0 | 1.67 |
| S(F125)_15 min. | 689.2 | 340.4 | 3.2 | 6.44 | 61.1 | 110.0 | 1.69 |

**Table 5**
$SSA_{BET}$ for paste-slag specimens.

| CP composition and treatment | $S_{BET}$ (m² g⁻¹) |
| --- | --- |
| C | 6.8 |
| C_10 min. | 20.1 |
| C + S(F < 63) | 14.3 |
| C + S(F < 63)_10 min. | 19.5 |
| C + S(F125) | 14.0 |
| C + S(F125)_10 min. | 29.6 |

was reacted in the cement matrix under PUS, showing improved pozzolanic reactivity of GBFS. A reduced CH content could also be associated with the formation of C-S-H richer in CaO due to PUS treatment, in more porous materials, the ingress of $CO_2$ is faster, so the conversion of $Ca(OH)_2$ into $CaCO_3$ could be faster. Similarly, Jiang et al. [50] noticed that the CH's peak intensity in the prepared specimens decreased significantly with an increase in GBFS. That's because the CH formed from clinker hydration was partially entangled in GBFS's pozzolanic reaction. Thus, the larger the GBFS content, the greater the CH consumption. It shows that a certain amount of GBFS participated in the pozzolanic reaction, leading to the reduction of CH and the creation of C-S-H.

### 3.5. XRD analysis

XRD analysis is an effective method for examining the phase composition of prepared specimens; however, in this study, it was used qualitatively. XRD patterns compiled in Fig. 9 pointed out the clear presence of a characteristic CH [50,55,56,63] ettringite [50,55,56,63], and C-S-H/C-A-S-H phase [50,55,56,63] in prepared specimens. Moreover, all prepared specimens presented almost identical XRD patterns, differing only in the intensity of the CH and C-S-H/C-A-S-H diffraction lines. Surprisingly, for the best-performing specimen ((C + S(F125)_10 min. – purple line) compared to the same specimen but prepared without PUS (blue line), there is an increase in intensity for C-S-H/C-A-S-H phase (diffraction peak at ~29.5°) and a decrease in intensity for CH (diffraction peaks at ~18° and ~34°), which may be linked to sonocrystalization of C-S-H/C-A-S-H seeds via pozzolanic interactions between GBFS and $Ca(OH)_2$. Additionally, some overlapping of the diffraction peaks of the alite and belite can be observed in the 2θ = 31.5°–33° range, indicating the development of C-S-H phases as alite and belite hydrate. This suggests that the short-term strength development of prepared CP specimens is caused by the alite phase's early hydration, whereas the belite phase contributes to the progressive enhancement of the long-term strength development.
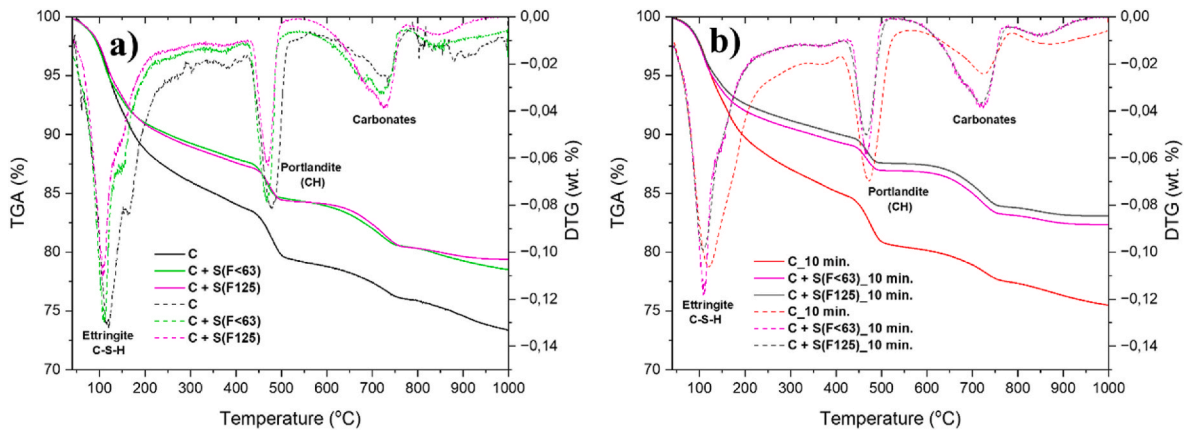
**Fig. 8.** TGA and DTG curves of C + S pastes prepared conventionally (a) and with the use of PUS (b), after 28 d.
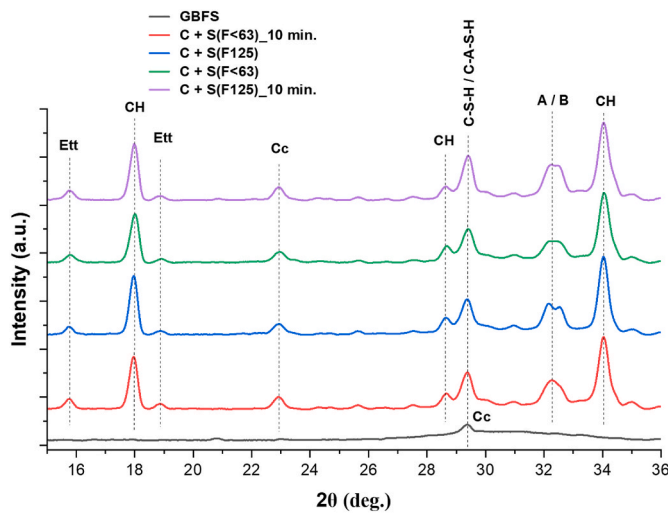


**Fig. 9.** XRD analysis of cement-GBFS paste specimens after 28 d(Ett – Ettringite, CH – Portlandite, A – Alite, B – Belite, Cc – Calcite).



**Fig. 10.** Laser granulometric particle size analysis of fractionated slag S(F125) subjected to PUS treatment.

### 3.6. Laser granulometric analysis (LG)

Laser granulometric (LG) particle size analysis was utilized to evaluate the particle size distribution (PSD) of the best-performing fraction of GBFS (125–250 µm) and check the influence of PUS on sonofragmentation (Fig. 10), which can reduce particle aggregation and enhance particle size refinement and tailoring shape. The duration of the PUS operation (from 5 to 15 min) influences the PSD (Table 4); it is reflected by an increase in $D_{50}$, an increase in the fine fraction, and a reduction in the coarse fraction of GFBS. The particle size changes after 15 min. PUS treatment would be explained by the particle re-agglomerating after de-agglomerating, especially at higher sonication power (100 % of amplitude), leading to partial connection of the GBFS particles because the ultrasonic cavitation causes large shockwaves and shear forces. PSD results provided proof of the detrimental impact of extended PUS treatment on the aggregation of mortar and cement pastes in the aqueous medium [33].

The specimens' span (Table 4), which is the width of the PSD mode based on 10, 50, and 90 % vol%, was computed using the following formula (3):

$$Span = \frac{D_{90} - D_{10}}{D_{50}} \quad (3)$$

The span factor suggests the overall idea of distribution width (uniformity) and the effectiveness of sonofragmentation of particle size,
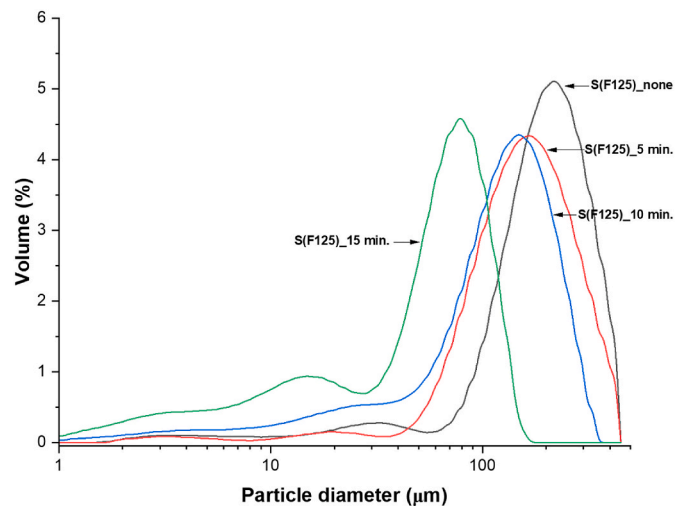
independent of the median size. A normal (Gaussian) distribution typically spans the range from 1 to 2. The results confirmed that the highest span value was obtained for C + S (F125)_10 min. among all the samples, which may indicate that 10 min. of PUS treatment is effective for sonofragmentation.

### 3.7. BET surface area analysis

Using the BET analysis, it is possible to ascertain how the PUS treatment may have affected the pore structure of the prepared specimens. $N_2$ adsorption-desorption isotherms for cement-slag paste C + S (F125) after 28 d are shown in Fig. 11a. According to the IUPAC classification [64], adsorption-desorption isotherms are of type IV/V, which is a feature of mesoporous material structure. Gas adsorption methods, such as nitrogen adsorption-desorption with the BET model, can be used to explore the $SSA_{BET}$ of cement-slag pastes (Table 5). The BJH model, among the indirect experimental methods [65], may be used for pore structure characteristics that correspond to the C-S-H interlayer spaces, the coexistence of adsorbed water phases, and small capillary pores [66].

Fig. 11a demonstrates that the adsorption/desorption amount of $N_2$ increases with relative pressure, and PUS treatment results in a larger adsorption amount of $N_2$. Due to PUS treatment, a major increase in $N_2$ accessible $SSA_{BET}$ was found: more than 100 % for C and (C + S(F125), while only 36 % for a small fraction of GFBS (Table 5). The higher
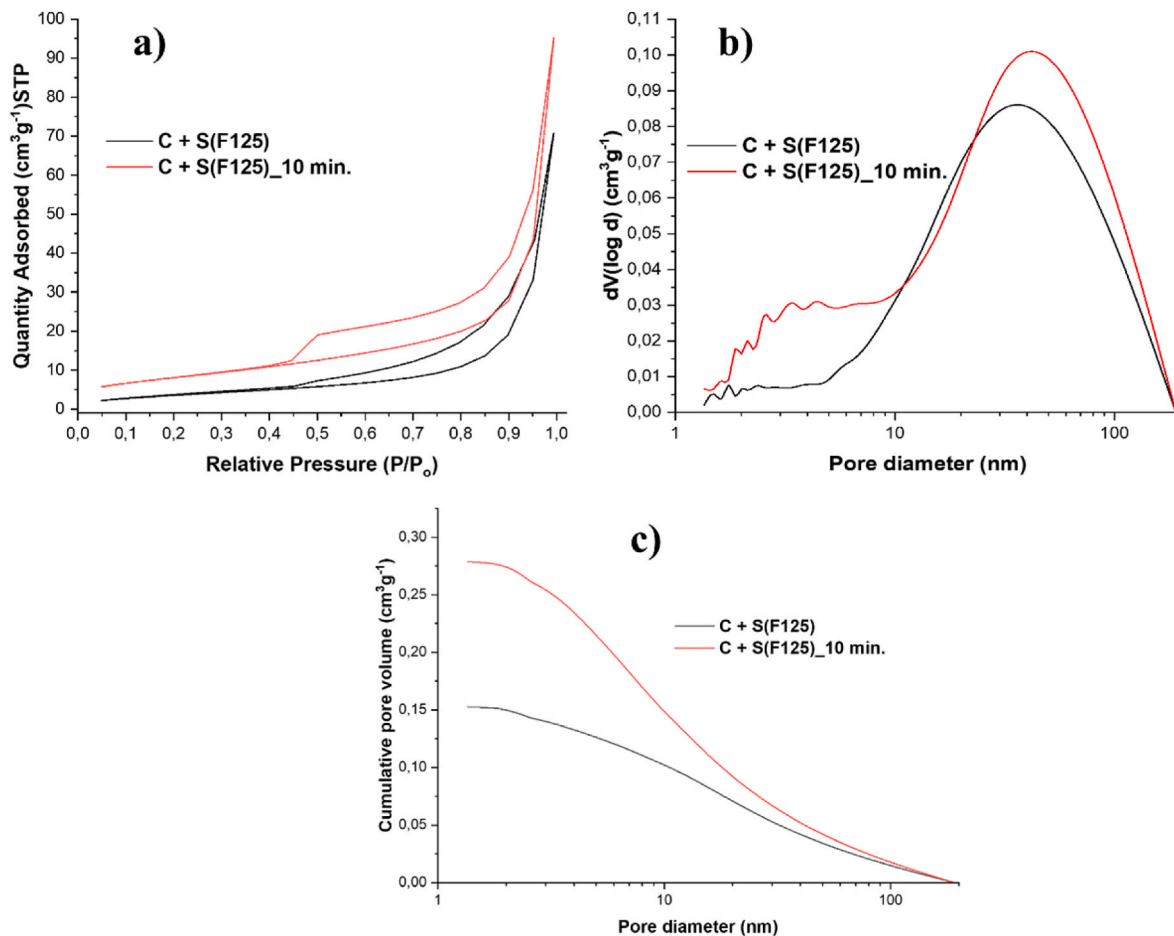
**Fig. 11.** $N_2$ adsorption-desorption isotherms (a), and PSD (b, c) for specimen C + S(F125) prepared under the influence of PUS and without PUS after 28 d.

$SSA_{BET}$ of the paste might be assigned to the ability of PUS treatment to produce some cracks and increase the mesoporous structure of slag and cement particles. It can also result in the formation of more surface active sites and reaction centers for sonocrystallization, as well as the creation of C-S-H/C-A-S-H nucleation seeds, which is valuable for enhancing physicochemical and mechanical performance.

According to Jiang et al. [67], the hysteresis between the sorption isotherms may be clarified by the collapse and resaturation of C-S-H interlayer seeds. Jiang et al. [50] observed that the structure of C-S-H, which was generated from cement and GBFS hydration, can modify pore structures. Fernandez [51] presented comparable adsorption-desorption isotherms, which were referred to as Type H3 (slit-shaped pore structure) isotherms, which may indicate the structure of C-S-H. The hysteresis's size and shape show a continuous distribution of pores that grew during hydration. The increase in C-S-H content caused by hydration evolution may increase $SSA_{BET}$. According to John et al. [68], C-S-H nucleation seeding during PUS treatment provides an exceptional opportunity for tailoring the size as well as further product control in seeded pastes. Ehsani et al. [33] discovered that PUS treatment does not influence the finer size fraction in aqueous suspension, implying that PUS treatment may be ineffective in disaggregating particles, especially those with a finer size, even after prolonged sonication times.

Figs. 11b and 11c display the PSD of a C + S(F125) paste specimen prepared under the influence of PUS and without PUS after 28 d, determined using the BJH model. A higher volume of small micropores (2–10 nm) was found in the PUS-treated paste in comparison to the reference paste. A shock wave caused by cavitation implosion may expand the aperture of the original pore (e.g., dilate or connect pores and microfractures), changing the crack network and establishing a new

equilibrium state according to adsorption-desorption kinetics. The observed PUS-induced micropore refinement could be linked to C-S-H interlayer spaces. Slag may refine nanopores, as Huang et al. [69] found by raising the volume of both small and large gel pores with interlayer-sized necks. Gel pores with a diameter of less than 10 nm can influence packing density and diversify mechanical properties. A decreased gel porosity is intended to result in improved mechanical properties, such as increased hardness and indentation modulus [70]. Higher w/c ratios (from 0.33 to 0.50) result in more capillary pores and fewer micropores (<2 nm) in pastes containing 50 % or more slag, according to BJH estimates [68].

### 3.8. FTIR analysis

FTIR spectra are provided in Fig. 12 to better illustrate the structural evolution of the hydrate phases and functional groups on the surface of prepared specimens. The bands in the range at 2358, 1440, and 884 $cm^{-1}$ are linked to the aliphatic compound's –C=O stretching [55, 71–73]. The peak at 3640 $cm^{-1}$ corresponds to CH [55,73,74]. The bands at 3435 and 1630 $cm^{-1}$ were connected to water's H-O-H bending vibrations [55,71,73,74]. The absorption peaks at 522, 930, and 1154 $cm^{-1}$ are characteristic absorption peaks of the –Si–O bond in the $SiO_2$ framework [71,73,74].

Surprisingly, after PUS treatment of the prepared specimen (C + S (F125)_10 min. – red line), the band intensity (see Appendix, Table A7) significantly increases (band observed at 2358 $cm^{-1}$) compared to the specimen prepared without PUS (green line). The intensity of this band can be dependent on the difference in the activation effect on GBFS in variant pH and age of curing, which can be strongly correlated with the
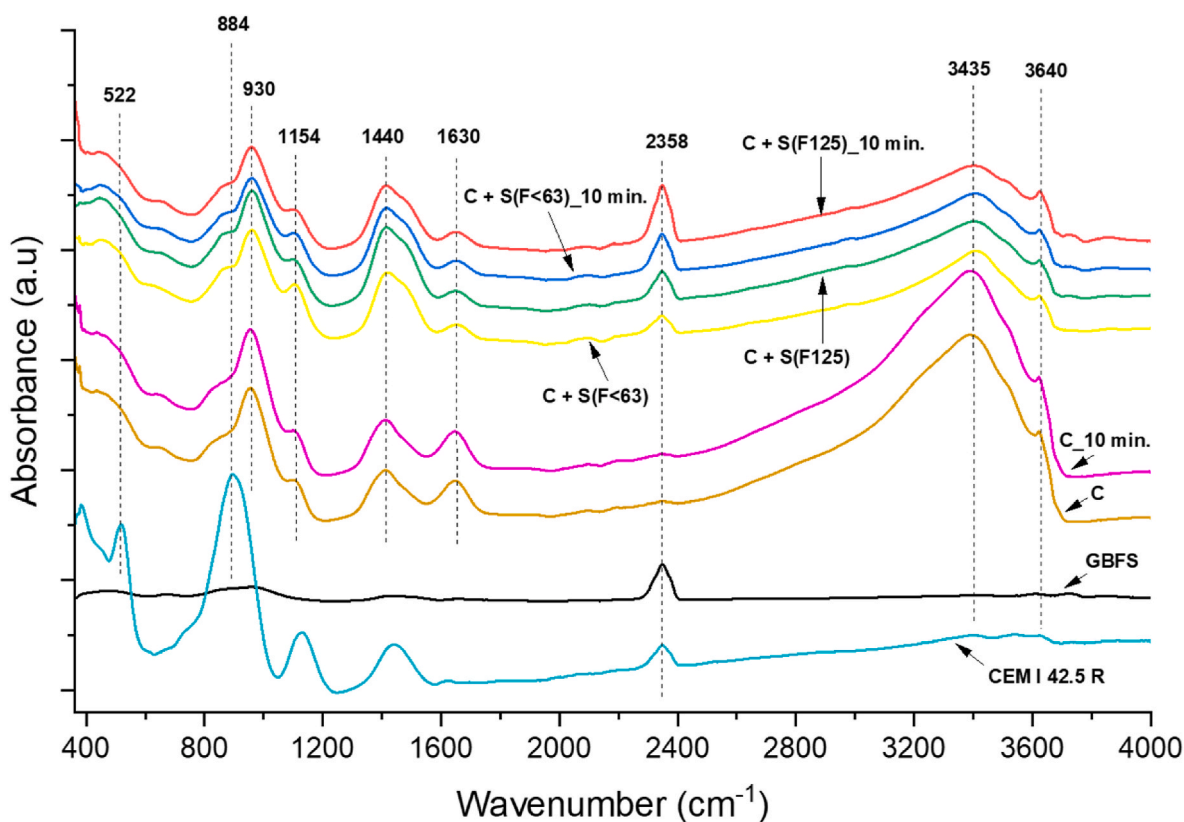
**Fig. 12.** The FTIR spectra for prepared specimens at 28 d and pure PC (CEM I 42.5R) and GBFS.

creation of C-S-H/C-A-S-H [71]. The cause for such a difference in intensity could be that PUS treatment may act as a "structure-directing factor" for the prepared specimen, and the "intimate" interface contact between cement and GBFS can be observed only with the participation of PUS treatment as an interfacial mediator. GBFS particles may well attach to the cement particles, which may be attributable to the sonocrystalization of C-S-H/C-A-S-H nucleation seeds (suggested by XRD and SEM images) via pozzolanic interactions between GBFS and CH (suggested by TGA analysis).

### 3.9. SEM with EDS

Figs. 13 and 14 show the morphologies of SEM images of paste specimens (C + S(F125)) prepared without PUS (Fig. 13) and under the influence of PUS (Fig. 14). EDS-spotting mode analysis was used to ascertain the hydration products' elemental compositions. After PUS treatment, the morphology of cement-GBFS paste was significantly different from the same specimen prepared without PUS. After sonication, GBFS particles were seen as irregular in shape with sharp edges, which are surrounded by white crystals formed during PUS treatment ("sonocrystals"). Additionally, PUS-induced dispersion of agglomerates/fragments or even inhibition of agglomeration can be observed; PUS seems to improve grain refinement and cause sonofragmentation of GBFS nucleant particles embedded in the cement matrix (Fig. 14).

EDS microanalysis was carried out to determine the elemental composition related to potential C-A-S-H nucleation seed growth. A comparison of EDS data for paste specimens prepared without PUS treatment (Fig. 13) and under PUS influence (Fig. 14) revealed a clear difference in Ca/Si and Al/Si ratios. There were, respectively, $1.3 \pm 0.01$ and $0.29 \pm 0.01$ for PUS-treated specimens and $2.1 \pm 0.02$ and $0.12 \pm 0.03$ for the reference specimens prepared conventionally. Such differences may indicate potential C-A-S-H sononucleation seeding. The following formula (4) was used to determine the maximum allowable

model alumina substitution into C-S-H during a pozzolanic reaction of GBFS pastes [75]:

$$\frac{Al}{Si} = \frac{1 - 0.4277\left(\frac{Ca}{Si}\right)}{4.732} \tag{4}$$

The results obtained by this formula confirmed that the maximum value (Al/Si) is respected for C + S(F125)_10 min. (Al/Si = 0.09) compared to the same specimen prepared without PUS treatment (Al/Si = 0.02).

### 3.10. The reaction mixture's pH

When C-A-S-H sononucleation seeds are formed, the reaction mixture's pH has a very important influence, and very high pH values (>13.0) in alkaline solutions may potentially activate the creation of C-A-S-H nucleates [76,77], which may promote the dissolution of the GBFS silicate glass network when polarized by highly reactive free radicals, particularly $OH^-$ radicals derived from PUS cavitation in aqueous solutions. To confirm this hypothesis, the reaction mixture's pH was measured before PUS and after 10 min (Table 6). Comparing cement-GBFS paste specimens prepared without PUS and under the influence of sonication, it can be stated that the reaction mixture's pH after PUS rises above 13.0, which may be another confirmation of C-A-S-H sononucleation seeding.

### 4. Discussion

The properties of deposited and fresh GBFS are expected to differ to some extent depending on the conditions and duration of storage [78]. After granulation, the slag is wet, is transported in wet conditions to the storage site, and remains mostly in a moist condition during storage, except for the surface layers that exhibit weather-related wetting and drying. Therefore, during storage, GFBS undergoes prehydration and
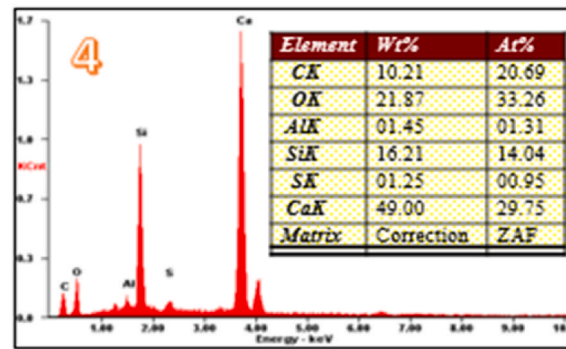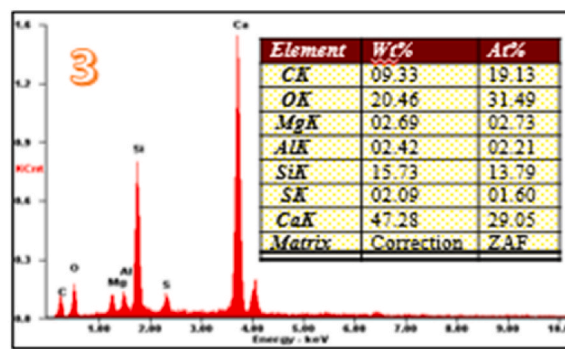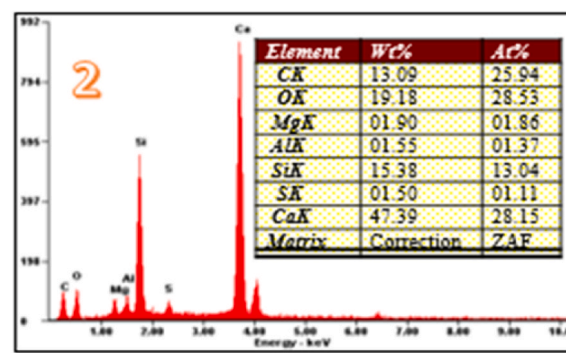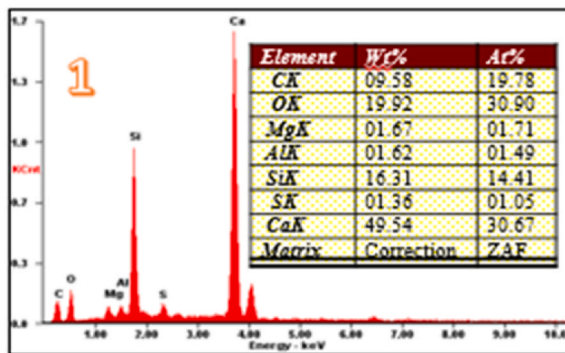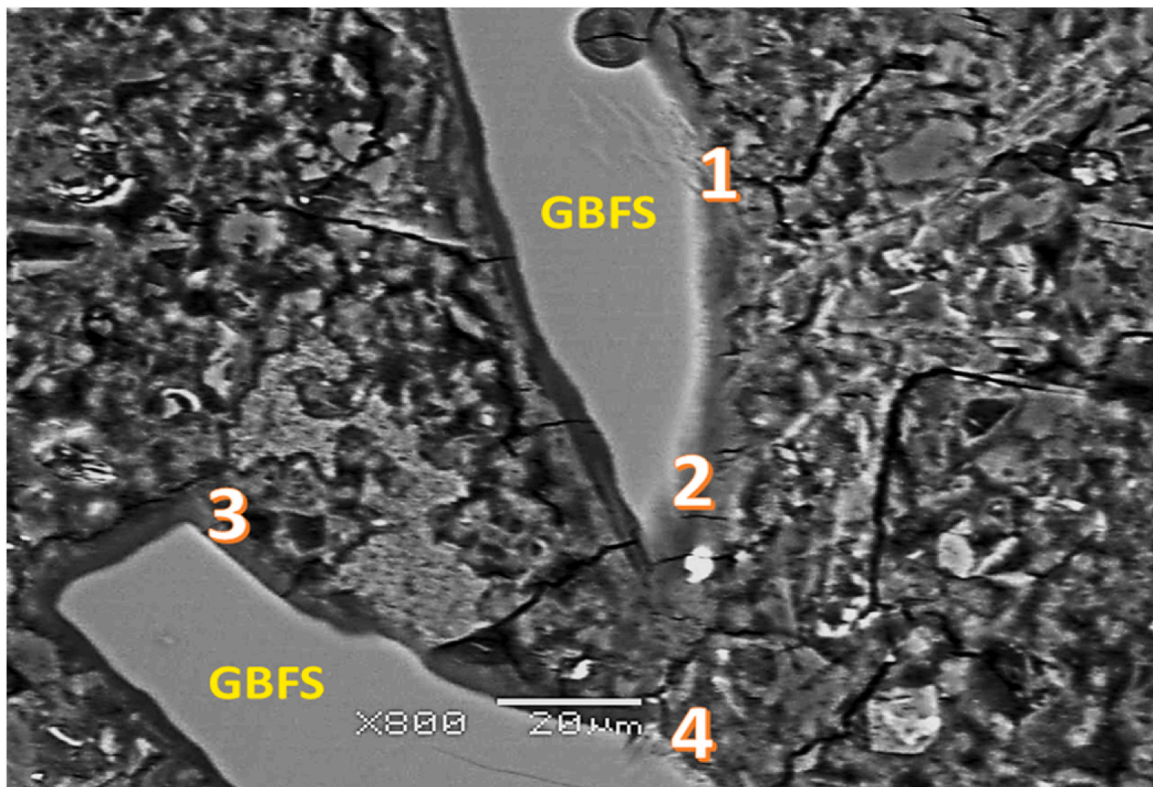
**Fig. 13.** SEM image of Cement-GBFS paste specimen C + S(F125) prepared without PUS at 28 d.

carbonation due to contact with atmospheric $CO_2$. These reactions are primarily caused by the fine fractions of GFBS [79]. These factors need to be considered when evaluating the results of the current investigation of fractionated GFBS.

Cement paste prepared without sonication revealed the expected reduction of both $f_c$ and $f_r$ when GFBS was used for the partial replacement of PC (Fig. 3). Such observed strength reduction is diminishing in curing time, as known from the literature [1–5]. Relative effects of fine (F < 63) and coarse (F125) fractions of slag could be controversial for fresh slag, but for deposited slag, they are well correlated with the observed presence of carbonation products on slag (the reflection of calcite in Fig. 9). A reduced reactivity of the fine fraction of slag (F < 63) due to prehydration and carbonation is also reflected by the rate of heat generated during the hardening of GFBS blended
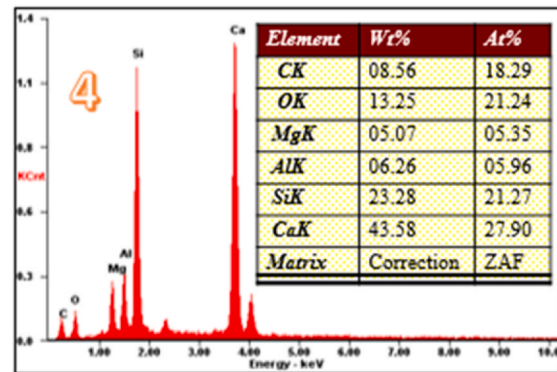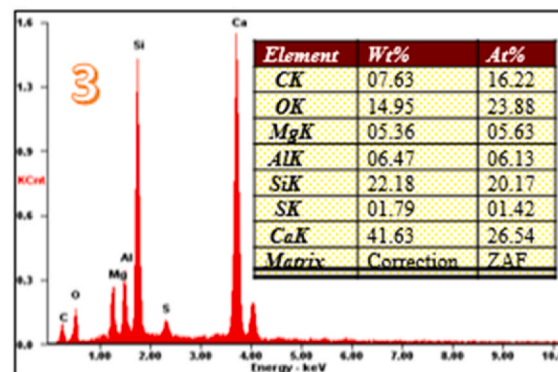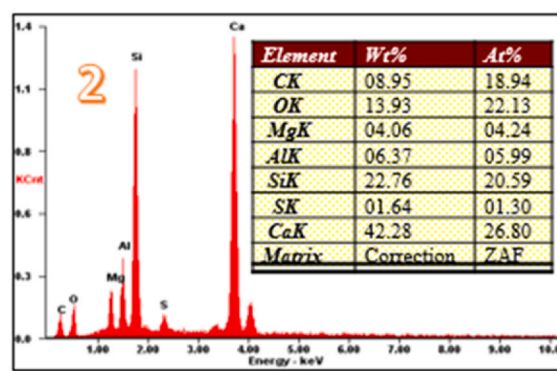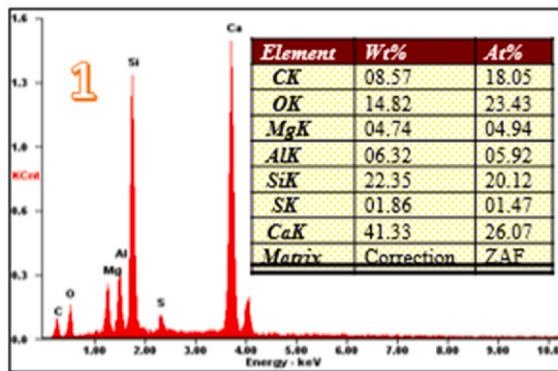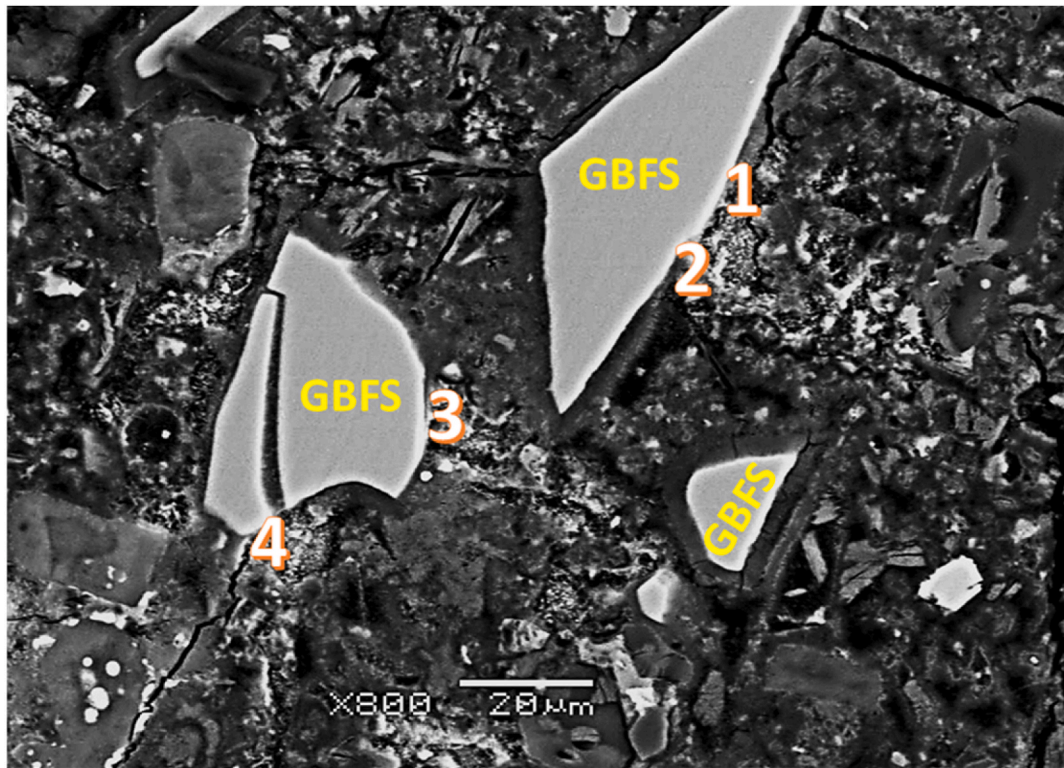
**Fig. 14.** SEM image of Cement-GBFS paste specimen C + S(F125) prepared under the influence of PUS at 28 d.

cement: the heat generated is quite close for (C + S(F < 63)) and (C + S (F125)), contrary to expectations for fresh GFBS. Substitute IS and FS times for cement pastes were extended for GFBS substituting cement, although the differences brought by different slag fractions were small.

PUS-induced effects on cement paste without GFBS, consisting of a relative increase in both $f_c$ and $f_r$, an increase in the heat of hardening, a decrease in the substitute IS and FS times, and an increase in the $SSA_{BET}$, coherently demonstrate accelerated cement hydration. The observed increase of the EM and VH follows the trends observed for the strength increase. The observed early strength increase was similar to that reported by Xiong et al. [36], but in contrast to a decrease in the 1-day strength of CP found by Ehsani et al. [33], who were using a higher

**Table 6**
The reaction mixture's pH measured before (initial) and after PUS treatment of cement paste.

| CP composition | C | C + S(F < 63) | C + S(F125) |
|---|---|---|---|
| Initial pH | 12.8 ± 0.1 | 12.8 ± 0.1 | 12.9 ± 0.1 |
| pH after PUS (10 min) | 12.9 ± 0.1 | 13.2 ± 0.1 | 13.4 ± 0.1 |

sonication frequency and sonication time of up to 10 min. The current investigation ranged the sonication time from 5 to 15 min and revealed the best PUS effects for 10 min.

The best performing cement-GBFS paste prepared by PUS demonstrated a remarkable improvement in $f_c$ and $f_r$ 2-day strengths (increase by 132 % and 58 %, respectively), major improvement of VH and EM (increase by 98 % and 74 %, respectively) in comparison to conventional mixing procedures. Similarly, an increase in SSA$_{BET}$ of about 111 %, a higher cumulative heat release of about 34 % after 2 days, reduced substitute setting times (IS by about 32 %, FS by about 55 %), and a reduction in CH content of about 29 % were observed. The PUS-treated cement-GBFS paste's 2-day strength matched that of the reference paste prepared without PUS. These results demonstrate strong accelerating effects of PUS treatment on cement-GFBS paste, much stronger than reported in the literature relative effects of PUS on cement paste without GFBS.

Any comparison of PUS-induced accelerating effects with known chemical activation methods for GFBS exceeds the scope of this investigation. Nevertheless, it's crucial to note that the commonly reported effects of GFBS in cementitious mixtures concern fresh, finely ground slag with a specific surface of at least 400–450 m$^2$ kg$^{-1}$ Blaine's, which is usually limited by energy-saving and economic considerations. Because GBFS has limited grindability and does not change significantly after storage [78], its grinding consumes electricity of around 65–69 kWh per ton [80], resulting in an environmental impact. Instead of grinding, in the current approach, slag particle separation was applied before PUS treatment, which allowed for the efficient utilization of rather coarse slag fractions.

The limitation of this study is the uncertain suitability of the PUS-treated cement + GBFS paste mixture for subsequent mixing with aggregate to produce concrete. To some limited extent, this concern was addressed by testing cement mortar with GFBS. According to the strength data presented in Table A5, the beneficial PUS-induced effects on the compressive and flexural strengths were partly retained; the relative strength improvement ranged from 35.9 % to 57.8 %, respectively. The best relative PUS-induced performance was noted for C + S (F125)_10 min mortar mixture, just as for paste mixtures.

## 5. Proposed formation mechanism of C-S-H/C-A-S-H nucleation seeding in the time of PUS treatment

The currently studied PUS treatment of cement-GFBS paste was mainly characterized by sonofragmentation (reduction of particle aggregation and enhanced size refinement of particles), consumption of CH, and potential C-S-H/C-A-S-H nucleation seeding. Mixing GFBS with cement paste may improve the composition of hydration products through PUS treatment, resulting in hardened specimens with superior physicochemical and mechanical properties. GFBS particles (especially 125–250 μm fraction) may be well bonded to products of cement hydration, which may have a strong link with the potential sonocrystalization of C-S-H/C-A-S-H nucleation seeds (suggested by XRD and SEM images (Fig. 14 and Fig. A2)) via pozzolanic interactions between GFBS and CH (suggested by TGA analysis).

PUS treatment accelerated the dissolution of Si$^{2+}$, Ca$^{2+}$, and Al$^{3+}$ ions, which may have helped C-S-H gels crystallize, according to Xiong et al. [81]. Particle size can significantly affect the microstructure, hydration kinetics, and mechanical characteristics of cement-based materials [51], and lattice and/or surface area distortions may decide the

dissolution peak. A particle's ability to dissolve seems to be highly influenced, regardless of its size, by the size of the other particles it is combined with. Regardless of size, a particle will act like a small one and dissolve sooner if the surrounding particles are larger, and act like a big one and dissolve later if the surrounding particles are smaller [51]. During the first deceleration period, particles with a higher SSA$_{BET}$ and defect concentration emit more heat. Let's suppose that only the dissolution of Si$^{4+}$ and Ca$^{2+}$ ions is responsible for the heat generated during the first peak. In that case, the amount of dissolved Ca$^{2+}$ ions throughout the process of hydration may be computed as a first step in a fairly straightforward way using the heat flows produced by each size of the particle. The idea that surface area influences reaction rate is supported by the fact that material dissolution and surface C-S-H nucleation regulate the initial reaction; therefore, a higher surface area would result in a faster reaction.

In light of this study's experimental findings and gained experience in the field of sonochemistry [38], it is allowed to develop a plausible reaction mechanism of C-S-H/C-A-S-H nucleation seeding in the time of PUS treatment for the best-performing specimen C + S(F125)_10 min. (Fig. 15). During initial PUS action on cement-slag water dispersion (pre-induction period, Fig. 5), collapse of inertial bubble implosions may result from initial sonofragmentation of previously agglomerated particles, therefore influencing the particle size through particle breakage and surface erosion phenomena (Stage Ia). A minimum particle size threshold is reached that depends on the frequency, initial particle size, and power is reached because the PUS treatment and particle breakage are limited. Specifically, the high power of PUS treatment can produce bigger bubbles that abruptly collapse, and produce powerful shockwaves. As a result, sonofragmentation is stronger and generally proportional to particle fineness.

Particle breakage may increase the solution's alkalinity and facilitate ion dissolution (Stage Ib). PUS treatment may efficiently disperse fragments and agglomerates or even inhibit agglomeration, improve grain refinement, and cause sonofragmentation of GBFS nucleant particles embedded in the cement matrix (as suggested by SEM images, Fig. 14). During the dissolution process, the chemical compounds of GBFS and cement particles will dissociate, forming ions for the PUS fragmentation process such as Ca$^{2+}$, Al$^{3+}$, and Si$^{4+}$, which may be triggered by pH change (from 12.8 to 13.4) as well as OH$^-$ owing to PUS treatment. It suggests that the overall trend is determined by the synergy between grain-size formation and PUS treatment. The increased alkalinity and PUS treatment may accelerate the disintegration of GBFS and cement particles, leading to the release of more ions and groups into the liquid phase. Consequently, more hydration products will be produced compared to specimens prepared without PUS.

In Stage IIa, the remaining Ca$^{2+}$ and OH$^-$ would continue to react to form Ca(OH)$_2$ during the early age of curing. In addition, with more CaO, Al$_2$O$_3$, and SiO$_2$ compositions in GBFS and cement particles (XRF analysis, Table 1), the reaction process will likely favour the hydration process forming hydrated calcium products, such as C-S-H/C-A-S-H seeds, and also induce a higher cumulative heat release. Since nucleation sites for PUS treatment are available as well as the increase in forming ion composition, the hydration process became rapid, and this was observed via a significantly decreasing FS time. As the amount of forming ions increases, polycondensation occurs, and a C-S-H/C-A-S-H seed may be formed.

In a later age of curing (Stage IIb), hydration products were accumulated, and the densely hardened cement paste's microstructure was developed, which is beneficial for strength development. The accelerated hydration of cement and slag, as well as the pozzolanic reaction, promote the hardening and densification of microstructure C + S(F125)_10 min. As a result, the 2-day $f_c$ reaches 20 MPa and the 28-day strength reaches 47 MPa, and these values well match the strength of reference cement paste. A major contribution to accelerated strength development is supposed to be because GBFS's pozzolanic reaction in cement paste has improved.
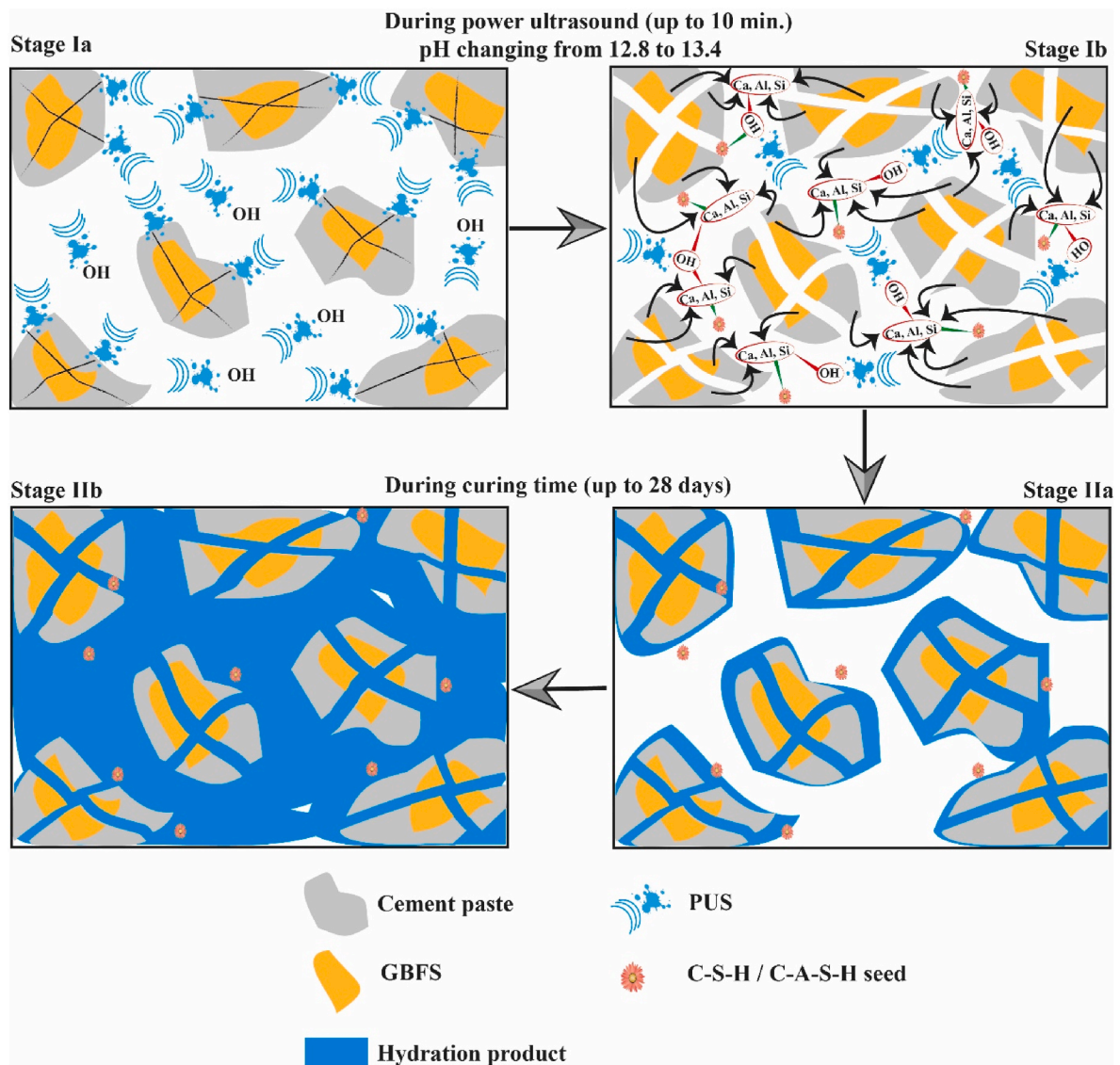
**Fig. 15.** Proposed reaction mechanism of C-S-H/C-A-S-H nucleation seeding in the time of PUS treatment for best-performing specimen C + S(F125)_10 min.

## 6. Conclusions

Using deposited and coarse granulated blast-furnace slag, this study comprehensively investigated the physicochemical and mechanical properties of cement-slag pastes treated with PUS under quasi-isothermal conditions. From the performed tests, the following conclusions can be drawn:

1. A small to moderate increase in $f_c$ and $f_r$ was found in Portland cement pastes treated with PUS (10 min) at the age of 2 days (up to 24 % and 7 %, respectively) to 28 days (up to 3 % and 9 %, respectively). The EM and VH increased similarly after receiving this PUS treatment, and the early rate of heat hydration increased as well.

2. PUS treatment of cement pastes containing 20 % of deposited GBFS resulted in considerably higher early strength ($f_c$ and $f_r$) after 2 days - up to 132 % and 58 %, respectively. The strength increase was correlated with increased cumulative heat of hardening. In a similar vein, following 28 days, the CH content dropped by 29 % while the VH and EM rose by 98 and 74 %, respectively.

3. Cement-GFBS paste specimens that underwent PUS treatment exhibited an increase of approximately 111 % in $N_2$ accessible $SS_{ABET}$ and an increase in pore volume within the 2–10 nm range according

to the BJH model. The best early-age strength and 28-day strength of paste were achieved with a 125–250 μm slag fraction thanks to the effective usage of relatively coarse slag fractions made possible by the combination of deposited slag particle separation and PUS treatment. With an increase in sonication time, there was a relative increase of fraction <63 μm and a drop of fraction >125 μm by 113 % and 81 %, respectively, in sonofragmentation of GBFS particles, particularly the 125–250 μm fraction.

The developed methodology for activation of deposited GFBS by particle separation and PUS treatment has several beneficial features, such as simplicity and proper temperature control with a specially designed sonoreactor. It shows the ability to increase the slag's reactivity in CP at room temperature, possibly via its ability to produce C-S-H/C-A-S-H sononucleation seeds. In that context, the results of this investigation could present new avenues for the development of new efficient procedures for the preparation of highly efficient cements with reduced clinker content.

## CRediT authorship contribution statement

**Paweł Lisowski:** Writing – original draft, Conceptualization, Data

curation, Formal analysis, Methodology, Validation, Visualization, Investigation, Writing – review & editing. **Daria Jóźwiak-Niedźwiedzka:** Investigation. **Magdalena Osial:** Investigation. **Kamil Bochenek:** Investigation. **Piotr Denis:** Investigation. **Michał A. Glinicki:** Conceptualization, Writing – review & editing, Supervision.

### Declaration of competing interest

The authors declare that they have no known competing financial interests or personal relationships that could have appeared to influence the work reported in this paper.

### Appendix

**Table A1**
Composition of the cement paste mixtures.

| Prepared specimens | Cement [g] | GBSF [g] | Water [g] | Actual acoustic energy [Joules]* |
|---|---|---|---|---|
| C | 450 | – | 225 | 72.5 ± 0.8 |
| C + S(F125) | 360 | 90 | 225 | 62.3 ± 0.9 |
| C + S(F < 63) | 360 | 90 | 225 | 56.1 ± 0.8 |

* Sonication conditions: ultrasonic horn tip (diameter of 25.4 mm), 20 kHz, 700 W, working at 100 % power of the generator) in continuous ultrasonic pulse mode (5s ON pulse time and 5s OFF - relaxation pulse time). Sonication in a vertical jacketed glass sonoreactor with the cooling system.

**Table A2** Composition of the cement paste mixtures subjected to PUS with and without cooling.

| Prepared specimens | Cement [g] | GBSF [g] | Water [g] | Mixture temperature without cooling [°C] | Mixture temperature with cooling [°C] |
|---|---|---|---|---|---|
| C_10 min. US | 450 | – | 225 | 47.8 ± 0.6 | 23.1 ± 0.4 |
| C + S(F125)_10 min. US | 360 | 90 | 225 | 49.4 ± 0.8 | 23.4 ± 0.7 |
| C + S(F < 63)_10 min. US | 360 | 90 | 225 | 48.7 ± 0.7 | 23.3 ± 0.5 |

**Table A2** $f_c$ and $f_r$ of cement-GBFS paste specimens.

| CP composition and PUS treatment * | $f_r$ [MPa] | | | $f_c$ [MPa] | | |
|---|---|---|---|---|---|---|
| | 2 days | 7 days | 28 days | 2 days | 7 days | 28 days |
| C + S(F < 63) | 2.1 ± 0.2 | 4.1 ± 0.3 | 6.1 ± 0.2 | 7.8 ± 0.4 | 16.8 ± 1.3 | 27.7 ± 1.0 |
| C + S(F63) | 2.7 ± 0.2 | 4.6 ± 0.5 | 6.5 ± 0.4 | 8.2 ± 0.5 | 17.8 ± 0.7 | 29.0 ± 1.1 |
| C + S(F125) | 3.0 ± 0.3 | 4.9 ± 0.4 | 6.7 ± 0.2 | 8.9 ± 0.6 | 19.9 ± 1.2 | 30.5 ± 1.1 |
| C + S(F < 63)_5 min. | 3.7 ± 0.1 | 5.7 ± 0.2 | 7.9 ± 0.5 | 11.7 ± 0.9 | 20.3 ± 1.6 | 29.3 ± 1.5 |
| C + S(F < 63)_10 min. | 4.1 ± 0.3 | 6.3 ± 0.5 | 8.5 ± 0.4 | 15.3 ± 0.7 | 23.3 ± 1.0 | 32.8 ± 1.6 |
| C + S(F < 63)_15 min. | 3.9 ± 0.3 | 6.1 ± 0.1 | 8.2 ± 0.3 | 14.3 ± 1.2 | 23.0 ± 1.7 | 32.5 ± 1.3 |
| C + S(F63)_5 min. | 4.1 ± 0.1 | 6.1 ± 0.3 | 8.0 ± 0.3 | 12.6 ± 1.1 | 22.0 ± 1.3 | 31.4 ± 1.4 |
| C + S(F63)_10 min. | 4.7 ± 0.1 | 6.7 ± 0.3 | 8.7 ± 0.4 | 16.5 ± 1.2 | 25.6 ± 1.2 | 34.6 ± 1.6 |
| C + S(F63)_15 min. | 4.4 ± 0.5 | 6.5 ± 0.3 | 8.6 ± 0.4 | 16.5 ± 1.2 | 25.6 ± 1.2 | 34.6 ± 1.6 |
| C + S(F125)_5 min. | 4.5 ± 0.3 | 6.3 ± 0.4 | 8.5 ± 0.4 | 15.4 ± 0.8 | 24.2 ± 1.4 | 33.5 ± 1.1 |
| C + S(F125)_10 min. | 4.9 ± 0.1 | 7.7 ± 0.3 | 10.1 ± 0.3 | 20.6 ± 0.6 | 33.2 ± 1.3 | 47.1 ± 1.2 |
| C + S(F125)_15 min. | 4.7 ± 0.3 | 7.5 ± 0.3 | 9.3 ± 0.2 | 18.5 ± 0.8 | 31.8 ± 1.5 | 43.9 ± 1.1 |

* Sonication conditions: ultrasonic horn tip (diameter of 25.4 mm), 20 kHz, 700 W, working at 100 % power of the generator) in continuous ultrasonic pulse mode (5s ON pulse time and 5s OFF - relaxation pulse time). Sonication in a vertical jacketed glass sonoreactor with the cooling system.

**Table A3**
$f_c$ and $f_r$ of cement-GBFS paste specimens.

| CP composition and PUS treatment * | $f_r$ [MPa] | | | $f_c$ [MPa] | | |
|---|---|---|---|---|---|---|
| | 2 days | 7 days | 28 days | 2 days | 7 days | 28 days |
| C + S(F < 63)_5 min. | 3.2 ± 0.2 | 5.0 ± 0.2 | 6.9 ± 0.5 | 11.2 ± 0.9 | 21.9 ± 1.1 | 31.0 ± 1.4 |
| C + S(F < 63)_10 min. | 3.4 ± 0.5 | 5.3 ± 0.3 | 7.7 ± 0.3 | 12.1 ± 1.3 | 22.8 ± 1.5 | 31.4 ± 1.5 |
| C + S(F < 63)_15 min. | 3.3 ± 0.1 | 5.1 ± 0.6 | 7.6 ± 0.2 | 12.0 ± 1.2 | 22.3 ± 1.1 | 31.1 ± 0.9 |
| C + S(F63)_5 min. | 3.7 ± 0.2 | 5.1 ± 0.1 | 7.4 ± 0.2 | 11.6 ± 0.7 | 22.8 ± 1.2 | 31.1 ± 1.7 |
| C + S(F63)_10 min. | 3.9 ± 0.3 | 6.7 ± 0.5 | 8.7 ± 0.4 | 14.0 ± 1.5 | 24.7 ± 1.5 | 33.1 ± 0.9 |
| C + S(F63)_15 min. | 3.8 ± 0.2 | 6.2 ± 0.2 | 8.1 ± 0.2 | 13.0 ± 1.4 | 23.7 ± 1.5 | 32.1 ± 1.5 |
| C + S(F125)_5 min. | 4.0 ± 0.3 | 5.4 ± 0.3 | 7.8 ± 0.6 | 12.0 ± 0.7 | 23.4 ± 1.5 | 33.4 ± 1.6 |
| C + S(F125)_10 min. | 4.3 ± 0.4 | 7.0 ± 0.3 | 9.0 ± 0.3 | 14.7 ± 1.3 | 27.9 ± 1.3 | 36.9 ± 1.0 |
| C + S(F125)_15 min. | 4.1 ± 0.4 | 6.5 ± 0.4 | 8.4 ± 0.3 | 13.7 ± 1.2 | 25.9 ± 1.3 | 35.9 ± 1.5 |

* GBFS treated by PUS and then mixed with cement to prepare specimens. Sonication conditions: ultrasonic horn tip (diameter of 25.4 mm), 20 kHz, 700 W, working at 100 % power of the generator) in continuous ultrasonic pulse mode (5s ON pulse time and 5s OFF - relaxation pulse time). Sonication in a vertical jacketed glass sonoreactor with the cooling system.

**Table A4**
Composition of the cement mortar mixtures and their consistency.

| Prepared specimens | Cement [g] | GBFS [g] | Water [g] | Sand [g] | Slump flow (mm) |
| --- | --- | --- | --- | --- | --- |
| C | 450 | – | 225 | 1350 | 173 ± 1.0 |
| C_10 min. US | | | | | 179 ± 1.0 |
| C + S(F125) | 360 | 90 | | | 128 ± 1.5 |
| C + S(F125)_10 min. US | | | | | 147 ± 1.5 |
| C + S(F < 63) | | | | | 123 ± 1.0 |
| C + S(F < 63)_10 min. US | | | | | 134 ± 1.5 |

**Table A5**
$f_c$ and $f_r$ of mortar specimens.

| Mortar designation and PUS treatment * | $f_r$ [MPa] | | | $f_c$ [MPa] | | |
| --- | --- | --- | --- | --- | --- | --- |
| | 2 days | 7 days | 28 days | 2 days | 7 days | 28 days |
| C | 5.7 ± 0.1 | 7.6 ± 0.1 | 9.3 ± 0.1 | 23.6 ± 0.9 | 36.8 ± 0.7 | 47.3 ± 0.9 |
| C_10 min. | 5.8 ± 0.1 | 7.6 ± 0.1 | 9.6 ± 0.1 | 28.7 ± 0.8 | 40.0 ± 0.8 | 49.4 ± 0.8 |
| C + S(F < 63) | 3.2 ± 0.2 | 4.8 ± 0.2 | 6.5 ± 0.1 | 13.3 ± 0.7 | 20.3 ± 0.6 | 29.6 ± 0.9 |
| C + S(F < 63)_10 min. | 4.7 ± 0.1 | 6.2 ± 0.1 | 7.8 ± 0.1 | 19.7 ± 0.9 | 31.3 ± 0.5 | 41.2 ± 0.9 |
| C + S(F125) | 3.9 ± 0.2 | 5.7 ± 0.1 | 7.6 ± 0.1 | 14.7 ± 0.8 | 22.7 ± 0.9 | 31.8 ± 0.8 |
| C + S(F125)_10 min. | 5.3 ± 0.1 | 7.3 ± 0.2 | 9.2 ± 0.1 | 23.2 ± 0.9 | 35.3 ± 0.5 | 45.5 ± 0.9 |

* Sonication conditions: ultrasonic horn tip (diameter of 25.4 mm), 20 kHz, 700 W, working at 100 % power of the generator) in continuous ultrasonic pulse mode (5s ON pulse time and 5s OFF - relaxation pulse time). Sonication in a vertical jacketed glass sonoreactor with the cooling system.
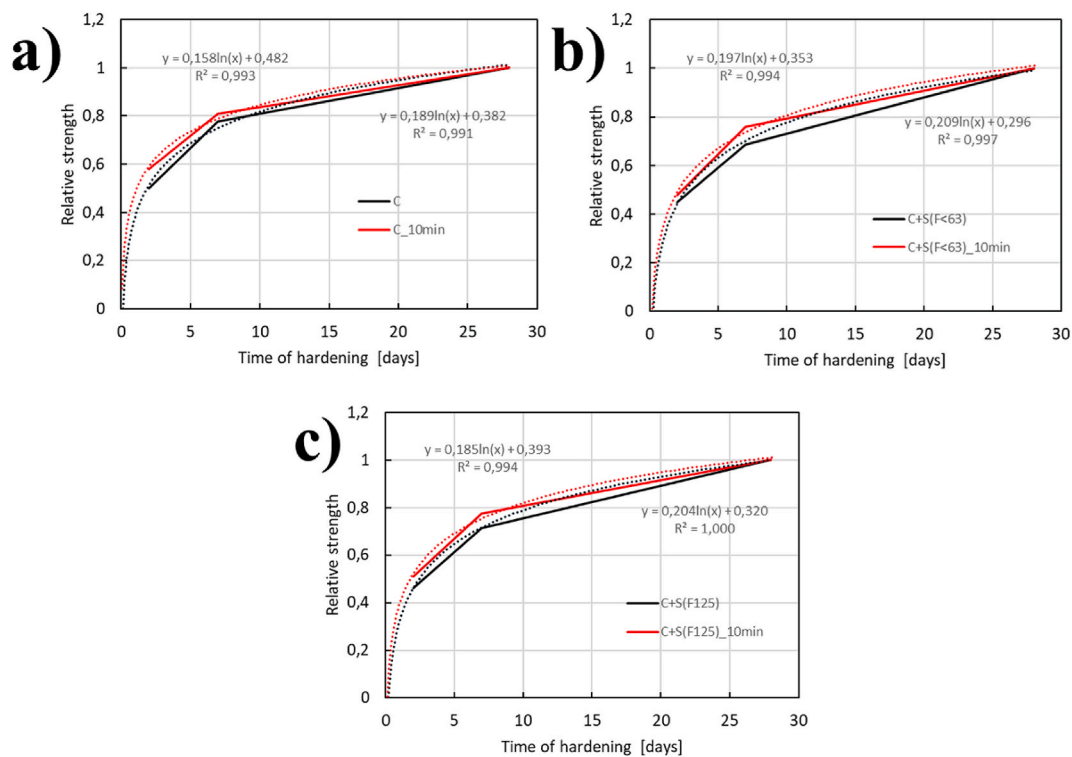


**Fig. A1.** The development of compressive strength of mortar specimens in time for three mortar compositions produced without or with 10 min pulse sonication.

The influence of PUS on the rate of early strength development is illustrated graphically by the shift of the red line above the black line. The PUS-induced shift can be numerically described by the parameters of the best-fit approximation formula shown in the figures.
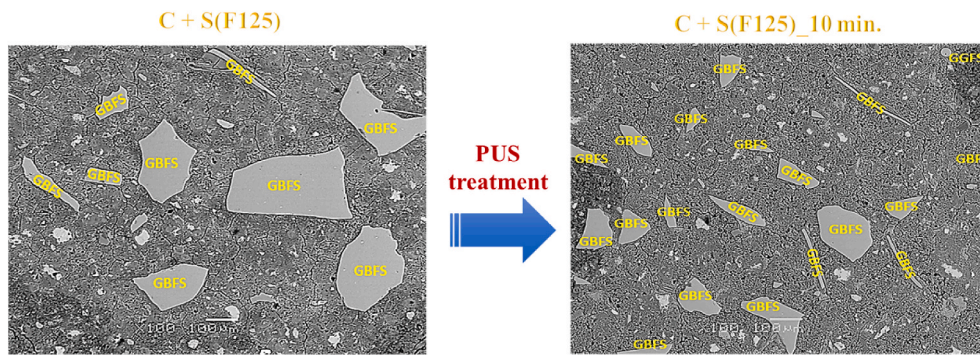
**Fig. A2.** SEM images of Cement-GBFS paste specimen C + S(F125) without PUS and under the influence of PUS at 28 d.

Data and peak analysis were obtained using the OriginPro® 2024 software package (Northampton, Massachusetts, USA).

**Table A6**
The Peak analysis of FTIR spectrum for cement-GBFS paste specimens at 28 d and GBFS and CEM I 42.5 R.

| CP composition and PUS treatment | Peak Analysis | |
|---|---|---|
| | (~2358) | |
| | Height of the Peak | Area of the Peak |
| GBFS | 0.0155 | 1.0384 |
| CEM I 42.5 R | 0.0095 | 0.6616 |
| C + S(F < 63) | 0.0077 | 0.5389 |
| C + S(F < 63)_10 min. | 0.0163 | 1.1033 |
| C + S(F125) | 0.0123 | 0.8358 |
| C + S(F125)_10 min. | 0.0250 | 1.6833 |

## Data availability

Data will be made available on request.

## References

[1] B. Lothenbach, K. Scrivener, R.D. Hooton, Supplementary cementitious materials, Cement Concr. Res. 41 (2011) 1244–1256, https://doi.org/10.1016/J.CEMCONRES.2010.12.001.

[2] M.C.G. Juenger, R. Snellings, S.A. Bernal, Supplementary cementitious materials: new sources, characterization, and performance insights, Cement Concr. Res. 122 (2019) 257–273, https://doi.org/10.1016/J.CEMCONRES.2019.05.008.

[3] Z. Giergiczny, Fly ash and slag, Cement Concr. Res. 124 (2019) 105826, https://doi.org/10.1016/J.CEMCONRES.2019.105826.

[4] W. Matthes, et al., Ground granulated blast-furnace slag, in: Nele De Belie, et al. (Eds.), Properties of Fresh and Hardened Concrete Containing Supplementary Cementitious Materials : State-Of-The-Art Report of the RILEM Technical Committee 238-SCM, vol. 25, Springer Nature, 2018, pp. 1–53, https://doi.org/10.1007/978-3-319-70606-1_1.

[5] H. Zhu, D.G. Mapa, C. Lucero, K.A. Riding, A. Zayed, Effect of slag characteristics on adiabatic temperature rise of blended concrete, ACI Mater. J. 119 (2022) 117–133, https://doi.org/10.14359/51733150.

[6] S. Li, C. Fu, W. Shi, Q. He, J. Wang, Chloride penetration in reinforced slag-based concrete beams under combined effects of loads and drying–wetting cycles, Mag. Concr. Res. 75 (2023) 1012–1026, https://doi.org/10.1680/jmacr.22.00331.

[7] C.C. Castellano, V.L. Bonavetti, H.A. Donza, E.F. Irassar, The effect of w/b and temperature on the hydration and strength of blastfurnace slag cements, Construct. Build. Mater. 111 (2016) 679–688, https://doi.org/10.1016/J.CONBUILDMAT.2015.11.001.

[8] M.Á. Sanjuán, E. Estévez, C. Argiz, D. del Barrio, Effect of curing time on granulated blast-furnace slag cement mortars carbonation, Cem. Concr. Compos. 90 (2018) 257–265, https://doi.org/10.1016/J.CEMCONCOMP.2018.04.006.

[9] M. Boháč, M. Gregerová, The influence of blast-furnace slag hydration products on microcracking of concrete, Mater. Char. 60 (2009) 729–734, https://doi.org/10.1016/J.MATCHAR.2008.11.011.

[10] Y. Briki, M. Zajac, M. Ben Haha, K. Scrivener, Factors affecting the reactivity of slag at early and late ages, Cement Concr. Res. 150 (2021) 106604, https://doi.org/10.1016/J.CEMCONRES.2021.106604.

[11] W. Chen, H.J.H. Brouwers, The hydration of slag, part 1: reaction models for alkali-activated slag, J. Mater. Sci. 42 (2007) 428–443, https://doi.org/10.1007/s10853-006-0873-2.

[12] M.J. McCarthy, T.D. Dyer, Pozzolanas and Pozzolanic Materials, Lea's Chemistry of Cement and Concrete, 2019, pp. 363–467, https://doi.org/10.1016/B978-0-08-100773-0.00009-5.

[13] M. Moranville-Regourd, S. Kamali-Bernard, Cements Made from Blastfurnace Slag, Lea's Chemistry of Cement and Concrete, 2019, pp. 469–507, https://doi.org/10.1016/B978-0-08-100773-0.00010-1.

[14] S. Adu-Amankwah, L. Black, L. Xianfeng, P. Hou, M. Zajac, Early age reaction of slag in composite cement: impact of sulphates and calcite, Cement 14 (2023) 100085, https://doi.org/10.1016/J.CEMENT.2023.100085.

[15] J. Skibsted, R. Snellings, Reactivity of supplementary cementitious materials (SCMs) in cement blends, Cement Concr. Res. 124 (2019) 105799, https://doi.org/10.1016/J.CEMCONRES.2019.105799.

[16] A. Schöler, F. Winnefeld, M. Ben Haha, B. Lothenbach, The effect of glass composition on the reactivity of synthetic glasses, J. Am. Ceram. Soc. 100 (2017) 2553–2567, https://doi.org/10.1111/jace.14759.

[17] K.C. Newlands, M. Foss, T. Matchei, J. Skibsted, D.E. Macphee, Early stage dissolution characteristics of aluminosilicate glasses with blast furnace slag- and fly-ash-like compositions, J. Am. Ceram. Soc. 100 (2017) 1941–1955, https://doi.org/10.1111/jace.14716.

[18] S. Kucharczyk, J. Deja, M. Zajac, Effect of slag reactivity influenced by alumina content on hydration of composite cements, J. Adv. Concr. Technol. 14 (2016) 535–547, https://doi.org/10.3151/jact.14.535.

[19] L. Steger, S. Blotevogel, L. Frouin, C. Patapy, M. Cyr, Experimental evidence for the acceleration of slag hydration in blended cements by the addition of CaCl2, Cement Concr. Res. 149 (2021) 106558, https://doi.org/10.1016/J.CEMCONRES.2021.106558.

[20] M. Whittaker, M. Zajac, M. Ben Haha, F. Bullerjahn, L. Black, The role of the alumina content of slag, plus the presence of additional sulfate on the hydration and microstructure of Portland cement-slag blends, Cement Concr. Res. 66 (2014) 91–101, https://doi.org/10.1016/J.CEMCONRES.2014.07.018.

[21] A. Bougara, C. Lynsdale, N.B. Milestone, Reactivity and performance of blast furnace slags of differing origin, Cem. Concr. Compos. 32 (2010) 319–324, https://doi.org/10.1016/J.CEMCONCOMP.2009.12.002.

[22] C. Xu, H. Li, X. Yang, Effect and characterization of the nucleation C-S-H seed on the reactivity of granulated blast furnace slag powder, Construct. Build. Mater. 238 (2020) 117726, https://doi.org/10.1016/J.CONBUILDMAT.2019.117726.

[23] E. Ganjian, A. Ehsani, T.J. Mason, M. Tyrer, Application of power ultrasound to cementitious materials: advances, issues and perspectives, Mater. Des. 160 (2018) 503–513, https://doi.org/10.1016/J.MATDES.2018.09.043.

[24] P. Lisowski, M.A. Glinicki, Novel processing methods of low-clinker multi-component cementitious materials—a review, Appl. Sci. 14 (2024), https://doi.org/10.3390/app14020899.

[25] E.D. Rodríguez, S.A. Bernal, J.L. Provis, J. Payá, J.M. Monzó, M.V. Borrachero, Structure of Portland cement pastes blended with sonicated silica fume, J. Mater. Civ. Eng. 24 (2012) 1295–1304, https://doi.org/10.1061/(ASCE)MT.1943-5533.0000502.

[26] D. Martínez-Velandia, J. Payá, J. Monzó, M. V Borrachero, Effect of sonication on the reactivity of silica fume in Portland cement mortars. https://doi.org/10.1680/ADCR.8.00027, 2015.

[27] A. Askarinejad, A.R. Pourkhorshidi, T. Parhizkar, Evaluation the pozzolanic reactivity of sonochemically fabricated nano natural pozzolan, Ultrason. Sonochem. 19 (2012) 119–124, https://doi.org/10.1016/J.ULTSONCH.2011.05.005.

[28] S. Peters, The influence of power ultrasound on setting and strength development of cement suspensions, PhD thesis, Bauhaus-Universität Weimar (2016). https://www.researchgate.net/publication/313613633_The_Influence_of_Power_Ultrasound_on_Setting_and_Strength_Development_of_Cement_Suspensions.

[29] A. Ehsani, E. Ganjian, T.J. Mason, M. Tyrer, M. Bateman, Insights into the positive effects of power ultrasound on the pore solution of Portland cement pastes, Cem. Concr. Compos. 125 (2022) 104302, https://doi.org/10.1016/J.CEMCONCOMP.2021.104302.

[30] Z. Xu, Y. Ji, Z. Ma, S. Xu, J. Zhang, Z. Zhang, Q. Xue, Strengthening mechanism of ultrasonic action on mechanical properties of cement-based materials, Construct. Build. Mater. 362 (2023) 129788, https://doi.org/10.1016/J.CONBUILDMAT.2022.129788.

[31] S. Peters, M. Kraus, C. Roßler, H.-M. Ludwig, Influence of power ultrasound on fluidity and microstructure of cement suspensions, in: Proceedings of the 13th International Conference on Cement Chemistry, 2011. https://www.researchgate.net/publication/289059774_Workability_of_cement_suspensions_Using_power_ultrasound_to_improve_cement_suspension_workability.

[32] G. Xiong, C. Wang, S. Zhou, Y. Zhao, Y. Li, Y. Liu, J. Qiu, Effect of power ultrasound-assisted mixing on the hydration and microstructural development of cement paste, J. Sustain. Cement-Based Mater. (2022) 1–12, https://doi.org/10.1080/21650373.2022.2153390.

[33] A. Ehsani, E. Ganjian, O. Haas, M. Tyrer, T.J. Mason, The positive effects of power ultrasound on Portland cement pastes and mortars; a study of chemical shrinkage and mechanical performance, Cem. Concr. Compos. 137 (2023) 104935, https://doi.org/10.1016/J.CEMCONCOMP.2023.104935.

[34] R. Remus, C. Rößler, H.-M. Ludwig, Power Ultrasound-Assisted Concrete Production-Workability, Strength Development, and Durability, ACI Sympos. Pub. 330 (n.d.). https://doi.org/10.14359/51711246.

[35] R. Remus, C. Rößler, S. Peters, T. Sowoidnich, H.M. Ludwig, Fundamental effects of using power ultrasound to accelerate $C_3S$ hydration, Cement Concr. Res. 180 (2024) 107514, https://doi.org/10.1016/J.CEMCONRES.2024.107514.

[36] G. Xiong, Y. Ren, X. Jia, Z. Fang, K. Sun, Q. Huang, C. Wang, S. Zhou, Understanding the influence of ultrasonic power on the hydration of cement paste, J. Build. Eng. 87 (2024) 108996, https://doi.org/10.1016/J.JOBE.2024.108996.

[37] R. Remus, C. Rößler, P. Hesse, S. Nune, H.-M. Ludwig, Power ultrasound assisted production of sustainable concrete, in: The 16th International Congress on the Chemistry of Cement, 2023. https://www.researchgate.net/publication/375602165_Power_ultrasound_assisted_production_of_sustainable_concrete.

[38] P. Lisowski, J.C. Colmenares, O. Mašek, W. Lisowski, D. Lisovytskiy, J. Grzonka, K. Kurzydłowski, Design and fabrication of $TiO_2$/lignocellulosic carbon materials: relevance of low-temperature sonocrystallization to photocatalysts performance, ChemCatChem 10 (2018) 3469–3480, https://doi.org/10.1002/CCTC.201800604.

[39] J.R.G. Sander, B.W. Zeiger, K.S. Suslick, Sonocrystallization and sonofragmentation, Ultrason. Sonochem. 21 (2014) 1908–1915, https://doi.org/10.1016/J.ULTSONCH.2014.02.005.

[40] X. Hangxun, B.W. Zeiger, K.S. Suslick, Sonochemical synthesis of nanomaterials, Chem. Soc. Rev. 42 (2013) 2555–2567, https://doi.org/10.1039/C2CS35282F.

[41] https://www.understanding-cement.com/bogue.html#:~:text=The%20Bogue%20calculation%20is%20used%20to%20calculate%20the,it%20can%20be%20adjusted%20for%20use%20with%20cement.

[42] T. Haneina, F.P. Glasserc, M.N. Bannerman, Thermodynamic data for cement clinkering, Cement Concr. Res. 132 (2020) 106043, https://doi.org/10.1016/j.cemconres.2020.106043.

[43] K. Kopecskó, A. Baranyi, K. Kopecskó, A. Baranyi, Comparative study of setting time and heat of hydration development of Portland cement according to EN 196-3, applications of calorimetry. https://doi.org/10.5772/INTECHOPEN.101912, 2022.

[44] M.A. Glinicki, A. Antolik, M. Gawlicki, Evaluation of compatibility of neutron-shielding boron aggregates with Portland cement in mortar, Construct. Build. Mater. 164 (2018) 731–738, https://doi.org/10.1016/J.CONBUILDMAT.2017.12.228.

[45] J. Bobrowicz, Study of cements initial setting time determination using curves of hydration rate evolution, measured by isometric calorimetry, Cement Wapno Beton 20 (2015) 401–410.

[46] M.A. Glinicki, M. Zielinski, Frost salt scaling resistance of concrete containing CFBC fly ash, Mater. Struct. 42 (2009) 993–1002, https://doi.org/10.1617/s11527-008-9438-y.

[47] R. Snellings, J. Chwast, Ö. Cizer, N. De Belie, Y. Dhandapani, P. Durdzinski, J. Elsen, J. Haufe, D. Hooton, C. Patapy, M. Santhanam, K. Scrivener, D. Snoeck, L. Steger, S. Tongbo, A. Vollpracht, F. Winnefeld, B. Lothenbach, RILEM TC-238 SCM recommendation on hydration stoppage by solvent exchange for the study of hydrate assemblages, Mater. Struct. 51 (2018) 172, https://doi.org/10.1617/s11527-018-1298-5.

[48] K. Scrivener, R. Snellings, B. Lothenbach, Thermogravimetric Analysis, A Practical Guide to Microstructural Analysis of Cementitious Materials, 2018, pp. 196–231, https://doi.org/10.1201/B19074-5.

[49] J.W. Bullard, H.M. Jennings, R.A. Livingston, A. Nonat, G.W. Scherer, J.S. Schweitzer, K.L. Scrivener, J.J. Thomas, Mechanisms of cement hydration, Cement Concr. Res. 41 (2011) 1208–1223, https://doi.org/10.1016/J.CEMCONRES.2010.09.011.

[50] W. Jiang, X. Li, Y. Lv, D. Jiang, Z. Liu, C. He, Mechanical and hydration properties of low clinker cement containing high volume superfine blast furnace slag and nano silica, Construct. Build. Mater. 238 (2020) 117683, https://doi.org/10.1016/J.CONBUILDMAT.2019.117683.

[51] M.M. Costoya Fernández, Effect of Particle Size on the Hydration Kinetics and Microstructural Development of Tricalcium Silicate, PhD Thesis, 2008, p. 234, https://doi.org/10.5075/epfl-thesis-4102.

[52] K.L. Scrivener, P. Juilland, P.J.M. Monteiro, Advances in understanding hydration of Portland cement, Cement Concr. Res. 78 (2015) 38–56, https://doi.org/10.1016/J.CEMCONRES.2015.05.025.

[53] A. Bazzoni, Study of early hydration mechanisms of cement by means of electron microscopy. https://api.semanticscholar.org/CorpusID:108968706, 2014.

[54] K. Scrivener, A. Ouzia, P. Juilland, A. Kunhi Mohamed, Advances in understanding cement hydration mechanisms, Cement Concr. Res. 124 (2019) 105823, https://doi.org/10.1016/J.CEMCONRES.2019.105823.

[55] G.H. Cai, Y.F. Zhou, J.S. Li, L.J. Han, C.S. Poon, Deep insight into mechanical behavior and microstructure mechanism of quicklime-activated ground granulated blast-furnace slag pastes, Cem. Concr. Compos. 134 (2022) 104767, https://doi.org/10.1016/J.CEMCONCOMP.2022.104767.

[56] X. Zhu, M. Vandamme, L. Brochard, Z. Zhang, Q. Ren, C. Li, B. He, H. Zhang, Y. Zhang, Q. Chen, Z. Jiang, Nature of aluminates in C-A-S-H: a cryogenic stability insight, an extension of DNA-code rule, and a general structural-chemical formula, Cement Concr. Res. 167 (2023) 107131, https://doi.org/10.1016/J.CEMCONRES.2023.107131.

[57] M. Saillio, V. Baroghel-Bouny, S. Pradelle, M. Bertin, J. Vincent, J.B. d'Espinose de Lacaillerie, Effect of supplementary cementitious materials on carbonation of cement pastes, Cement Concr. Res. 142 (2021) 106358, https://doi.org/10.1016/J.CEMCONRES.2021.106358.

[58] O.R. Ogirigbo, L. Black, Influence of slag composition and temperature on the hydration and microstructure of slag blended cements, Construct. Build. Mater. 126 (2016) 496–507, https://doi.org/10.1016/J.CONBUILDMAT.2016.09.057.

[59] E.D. Rodríguez, L. Soriano, J. Payá, M.V. Borrachero, J.M. Monzó, Increase of the reactivity of densified silica fume by sonication treatment, Ultrason. Sonochem. 19 (2012) 1099–1107, https://doi.org/10.1016/J.ULTSONCH.2012.01.011.

[60] X.M. Aretxabaleta, J. López-Zorrilla, C. Labbez, I. Etxebarria, H. Manzano, A potential C-S-H nucleation mechanism: atomistic simulations of the portlandite to C-S-H transformation, Cement Concr. Res. 162 (2022) 106965, https://doi.org/10.1016/J.CEMCONRES.2022.106965.

[61] S. Barzgar, M. Tarik, C. Ludwig, B. Lothenbach, The effect of equilibration time on Al uptake in C-S-H, Cement Concr. Res. 144 (2021) 106438, https://doi.org/10.1016/J.CEMCONRES.2021.106438.

[62] I.G. Richardson, The calcium silicate hydrates, Cement Concr. Res. 38 (2008) 137–158, https://doi.org/10.1016/J.CEMCONRES.2007.11.005.

[63] R. Maddalena, K. Li, P.A. Chater, S. Michalik, A. Hamilton, Direct synthesis of a solid calcium-silicate-hydrate (C-S-H), Construct. Build. Mater. 223 (2019) 554–565, https://doi.org/10.1016/J.CONBUILDMAT.2019.06.024.

[64] M.A. Al-Ghouti, D.A. Da'ana, Guidelines for the use and interpretation of adsorption isotherm models: a review, J. Hazard Mater. 393 (2020) 122383, https://doi.org/10.1016/J.JHAZMAT.2020.122383.

[65] Z.L. Jiang, Y.J. Pan, J.F. Lu, Y.C. Wang, Pore structure characterization of cement paste by different experimental methods and its influence on permeability evaluation, Cement Concr. Res. 159 (2022) 106892, https://doi.org/10.1016/J.CEMCONRES.2022.106892.

[66] N. De Belie, J. Kratky, S. Van Vlierberghe, Influence of pozzolans and slag on the microstructure of partially carbonated cement paste by means of water vapour and nitrogen sorption experiments and BET calculations, Cement Concr. Res. 40 (2010) 1723–1733, https://doi.org/10.1016/J.CEMCONRES.2010.08.014.

[67] Z. Jiang, Y. Xi, X. Gu, Q. Huang, W. Zhang, Modelling of water vapour sorption hysteresis of cement-based materials based on pore size distribution, Cement Concr. Res. 115 (2019) 8–19, https://doi.org/10.1016/J.CEMCONRES.2018.09.015.

[68] E. John, T. Matschei, D. Stephan, Nucleation seeding with calcium silicate hydrate – a review, Cement Concr. Res. 113 (2018) 74–85, https://doi.org/10.1016/J.CEMCONRES.2018.07.003.

[69] L. Huang, L. Tang, L. Wadsö, I. Löfgren, N. Olsson, Z. Yang, Using water vapour and $N_2$ isotherms to unveil effects of SCMs on nanopores and evaluate hydration degree, Cement Concr. Res. 164 (2023) 107042, https://doi.org/10.1016/J.CEMCONRES.2022.107042.

[70] X. Zhu, L. Brochard, M. Vandamme, Q. Ren, C. Li, Z. Jiang, A hierarchical C-S-H/ organic superstructure with high stiffness, super-low porosity, and low mass density, Cement Concr. Res. 176 (2024) 107407, https://doi.org/10.1016/J.CEMCONRES.2023.107407.

[71] G. Sun, J. Zhang, N. Yan, Microstructural evolution and characterization of ground granulated blast furnace slag in variant pH, Construct. Build. Mater. 251 (2020) 118978, https://doi.org/10.1016/J.CONBUILDMAT.2020.118978.

[72] A. Bouaziz, R. Hamzaoui, S. Guessasma, R. Lakhal, D. Achoura, N. Leklou, Efficiency of high energy over conventional milling of granulated blast furnace slag powder to improve mechanical performance of slag cement paste, Powder Technol. 308 (2017) 37–46, https://doi.org/10.1016/J.POWTEC.2016.12.014.

[73] P.A. Bhat, N.C. Debnath, Theoretical and experimental study of structures and properties of cement paste: the nanostructural aspects of C–S–H, J. Phys. Chem. Solid. 72 (2011) 920–933, https://doi.org/10.1016/J.JPCS.2011.05.001.

[74] J. Higl, D. Hinder, C. Rathgeber, B. Ramming, M. Lindén, Detailed in situ ATR-FTIR spectroscopy study of the early stages of C-S-H formation during hydration of monoclinic C3S, Cement Concr. Res. 142 (2021) 106367, https://doi.org/10.1016/J.CEMCONRES.2021.106367.

[75] M. Saillio, V. Baroghel-Bouny, M. Bertin, S. Pradelle, J. Vincent, Phase assemblage of cement pastes with SCM at different ages, Construct. Build. Mater. 224 (2019) 144–157, https://doi.org/10.1016/J.CONBUILDMAT.2019.07.059.

[76] M. Kovtun, E.P. Kearsley, J. Shekhovtsova, Chemical acceleration of a neutral granulated blast-furnace slag activated by sodium carbonate, Cement Concr. Res. 72 (2015) 1–9, https://doi.org/10.1016/J.CEMCONRES.2015.02.014.

[77] S. Song, H.M. Jennings, Pore solution chemistry of alkali-activated ground granulated blast-furnace slag, Cement Concr. Res. 29 (1999) 159–170, https://doi.org/10.1016/S0008-8846(98)00212-9.

[78] A. Ehrenberg, Does stored granulated blast furnace slag lose its reactivity? Cement Int. 10 (4) (2012) 64–79. https://www.researchgate.net/publication/287068348_Does_stored_granulated_blastfurnace_slag_lose_its_reactivity.

[79] A. Ehrenberg, Stored granulated blast furnace slag: grindability and reactivity - Global Slag Conference 2018, Presentation given at the Global Slag Conference & Exhibition in Prague on 24 - 24 April 2018. https://www.youtube.com/watch?v=Hb1Lsqc6FJw.

[80] D.S. Fortsch, Wear impacts in slag grinding in various grinding technologies, in: Conference Record Cement Industry Technical Conference, 2005., 2005, pp. 177–191, https://doi.org/10.1109/CITCON.2005.1516360.

[81] G. Xiong, C. Wang, S. Zhou, Y. Zheng, Y. Ren, Z. Fang, Y. Zhao, Understanding the thermal effect of power ultrasound in cement paste, Appl. Therm. Eng. 232 (2023) 120946, https://doi.org/10.1016/J.APPLTHERMALENG.2023.120946.